Synergistic reinforcement of Cu/Ti_3SiC_2/C laminated-like composites with the bimodal and highly oriented graphite flake and graphene nanoplatelets

Mu Wang[1,2], Xiaosong Jiang[1,2], Hongliang Sun[1,2], Zixuan Wu[3], Liu Yang[4]*

[1]Key Laboratory of Advanced Technologies of Materials, Ministry of Education, Chengdu 610031, China

[2]School of Materials Science and Engineering, Southwest Jiaotong University, Chengdu Sichuan 610031, China

[3]School of Engineering and Materials Science, Queen Mary University of London, London E1 4NS, United Kingdom

[4]Institute for Applied Materials (IAM-WK), Karlsruhe Institute of Technology (KIT), Karlsruhe 76131, Germany

***Corresponding author**: xsjiang@swjtu.edu.cn **(X.S. Jiang)**

Abstract

This study describes the preparation of bimodal reinforced Cu/Ti_3SiC_2/C laminated-like composites using flake powder metallurgy and vacuum hot-press sintering process. The objective was to accurately modulate the formation of oriented reinforcement network in two-dimensional carbon materials. The powders used in the five designed composites were flake Cu powder (45-60 μm), Ti_3SiC_2 (1-5 μm), graphite flakes (GFs, 120 μm) and graphene nanoplatelets (GNPs, 15 μm). Among them, the proportions of

Ti_3SiC_2 (10 wt %) and GFs (3 wt %) remained unchanged, GNPs accounted for 0 wt %, 0.5 wt %, 1.0 wt %, and 1.5 wt %, and Cu powder accounted for a decreasing proportion. Formation mechanisms of GFs and GNPs in oriented networks were quantitatively analyzed using the alignment model. Additionally, the related strengthening and failure mechanisms were investigated. According to the study, the bimodal laminated-like $Cu/Ti_3SiC_2/C$ composites with 0.5 wt% GNPs added showed the best overall performance. Specifically, it exhibited a hardness of 125.7 HV, tensile strength of 276.3 MPa, thermal conductivity of 207.8 $W \cdot m^{-1} \cdot K^{-1}$, and electrical conductivity of 23.6 MS/m. The network enhanced by the two-dimensional carbon material achieves efficient and orderly load transfer and dissipation mechanisms, optimizing stress distribution and enhancing fracture resistance, resulting in improved mechanical properties. In addition, the formation of the oriented reinforcement network optimizes the orientation arrangement of the reinforcing particles, which somewhat mitigates the scattering of thermoelectric carriers by structural defects in the composites, and the enlarged mean free-range improves the migration efficiency of electrons and phonons. Therefore, the erection of bimodal laminated-like structure achieves the goal of optimizing the properties of the composites.

Keywords

Powder metallurgy; Ball milling; Nanocomposites; Electrical properties; Thermal properties; Bimodal laminated-like structure.

1. Introduction

Metal matrix composites (MMCs) employ metals or alloys as the matrix and utilize reinforcement engineering embedded in single-phase or multiphase reinforcing materials to diversify the structural functions[1]. The design of the composite structure and the combination of reinforcing materials in MMCs is important factors in reinforcement engineering，which objective is to improve the performance of the composite material beyond that of its individual components[2]. By carefully selecting, arranging and fine-tuning the reinforcing materials in the matrix, it is possible to design composites with excellent overall properties[3]. Carbon nano-reinforcements such as carbon fibers, carbon nanotubes, graphene, and activated carbon are widely used in metal matrix composites due to their outstanding strength, stiffness, low density, and excellent thermal conductivity (TC) and electrical conductivity (EC)[4]. Among them，the two-dimensional carbon material GNPs and their multilayer stacked products, GFs, both exhibit superior mechanical, electrical, and thermal enhancement benefits thanks to the sp^2 hybridization of the carbon atoms, the strong covalent C-C bonding, and the hard lattice structure that is easy to be traversed by phonons, which make them promise materials for enhancing the performance of MMCs[5-7]. However, the strengthening effect of GFs and GNPs in metal matrix composites is often lower than expected due to their ease of agglomeration, haphazard orientation, and interfacial mismatch with the matrix. These factors lead to an increase in structural defects and a decrease in the efficiency of load transfer in the composites[8-10]. Therefore, it is necessary to promote the uniform dispersion and directional distribution of 2D carbon materials by optimizing the process.

The incorporation of nanoscale carbonaceous materials as reinforcing phases in carbon nano-reinforced Cu matrix composites results in the delivery of excellent overall performance[11, 12]. The performance guarantee is contingent upon the establishment of robust interfacial bonding and the optimal distribution of the Cu matrix and the carbon phase[13]. Fortunately, a number of techniques are available to achieve this objective. For instance, in the development of Cu/Ti_3SiC_2/C composites, researchers have utilized surface modification and distributed ball-milling mixing to effectively address the agglomeration issue of 2D carbon materials. The well-dispersed Ti_3SiC_2, GFs, and GNPs have resulted in improved mechanical and electrical properties through multiphase synergistic reinforcement at the micro- and nanoscale[14-16]. Among them, Ti_3SiC_2 has self-lubricating properties and can undergo elemental diffusion and interfacial reaction with Cu under high-temperature driving force, resulting in strong interfacial bonding，which improves the hardness and electrical properties of composites[17, 18]. GFs particles utilize their flake structure to provide effective parallel interfaces in the matrix and undergo micro-pitch planar slip under stress, which is beneficial to tuning crack trajectories and dissipating fracture energy[19]. In addition, small-particle GNPs have easy curling properties and are immobilized at the boundary or interface of matrix grains under stress. This allows them to bear high loads and build high-flux thermoelectric carrier channels, demonstrating the multi-functionalization of MMCs[20, 21]. However, if the co-doping content of GFs and GNPs exceeds a certain threshold, they will adsorb each other and form aggregation zones and interlayer slips. This can cause inconsistent

responses to residual stress release during deformation, leading to localized stress concentration. Furthermore, the existence of disordered orientation and interfacial defects in GFs and GNPs generates areas of thermoelectric carrier scattering, which decreases the energy transfer efficiency[22]. Utilizing the respective characteristics of GFs and GNPs to form specific network structures can significantly reduce the impact of these negative factors. Therefore, to obtain high-performance co-reinforced metal composites with GFs and GNPs, it is crucial to optimize the distribution strategy of 2D carbon particles to achieve their high alignment and improved interactions.

In fact, the structure of highly aligned and oriented assembly of enhanced phases is inspired by the laminated organization of pearl oysters. This structure is assembled by layering the soft and hard phases at multiple scales, resulting in a highly dispersed, highly aligned, and ordered distribution of enhancement phases[23, 24].The distribution of reinforcing phases in Cu/Ti_3SiC_2/C composites is ordered to effectively manage and disperse stresses, preventing localized strain concentration and inhibiting crack nucleation[25].GFs and GNPs of varying sizes and dimensions can connect at matrix defects to form a three-dimensional percolation network[22, 26]. This three-dimensional network can effectively reduce the phonon scattering and increase the mean free range of phonons, which is like building many efficient thermal and electrical conductive paths in the matrix, thus optimizing the thermal and electrical conduction efficiency of composites [27]. Therefore, designing bionic laminated structures is a good strategy for achieving the orderly assembly of enhanced phases at the micro and nanoscale. In MMCs, specific

geometrical arrangements or special designs in the material are typically achieved through the use of specialized fabrication methods that allow precise control of the distribution and orientation of the reinforcement. Currently, the most commonly used processes include magnetic field guided, theologically guided, self-assembly, and co-stretching[28, 29]. However, it must be recognized that single methods may have inherent drawbacks. For instance, Zhong et al. constructed Cu/Al laminate alloy plates using a flat surface roll bonding process, which demonstrated a combined enhancement in strength and toughness[30]. However, conventional cold flat rolling is challenging to achieve high-quality interfacial bonding, and there are significant differences in stacking fault energies. Zhou et al. constructed long-range ordered Cu/Al laminated alloy plates by electric pulse-assisted ultrasonic additive manufacturing, which resulted in high-quality interfacial bonding[31]. However, additive manufacturing presents limitations, including material and size constraints, which impede its applicability in specific scenarios. Therefore, the process should be optimized by a stepwise composite approach. Flake powder metallurgy (FPM) is a process that combines self-assembly and rheology guidance to build laminated structures， which process achieves precisely oriented assembly of multi-scale structures through material adaptability and matrix flow-assisted guided self-assembly[32, 33]. FPM can enhance the geometrical compatibility between the matrix and reinforcement by utilizing the high plasticity of the Cu matrix. This is achieved by creating large surface area adsorption planes through high-energy ball milling, which induces the attachment of GFs and GNPs[23, 28]. During the powder

assembly process, the GFs and GNPs located between the Cu flakes are self-oriented under gravity to form a laminated structure. The flow of semi-molten Cu, which is guided by the vacuum hot press sintering (VHPs), facilitates the planar orientation of the reinforcing phases and the alignment process. Furthermore, the application of unidirectional high pressure promotes the planar orientation of the reinforcing phases and facilitates the alignment process. GFs and GNPs with different size dimensions have size bimodal reinforcement properties, which are distributed parallel or overlapped or interlaced at the particle boundaries of the Cu matrix, thus forming a bimodal particle-reinforced laminated structure conducive to supporting cracks and deformations[34, 35].

This study prepared bimodal reinforced Cu/Ti_3SiC_2/C laminated-like composites with varying GNPs contents using FPM and VHPs composite process. The effect of GNPs content on the laminated-like composites was analyzed by comparing the differences in morphology and properties of composites with different structures. The bimodal laminated-like structure design optimizes the comprehensive performance of the composites. The study aims to provide new insights for the preparation of reinforced, phase-controllable, highly oriented laminated-like composites.

2. Experimental procedure

2.1 Preparation of raw materials

The initial microscopic morphology of the three reinforcing particles used in this study is shown in Fig. 1. The powder of GFs has an average diameter of approximately 120 μm and a thickness of around 10 μm. The powder of GNPs has an average diameter

of approximately 15 μm and a thickness of around 20 nm. The GFs were immersed in an aqueous solution of sodium dodecyl sulfate(SDS) and stirred for 30 min. Similarly, the GNPs were immersed in an aqueous solution of Rutin and stirred for 20 min to obtain well-dispersed reinforced particles. The initial Cu powder is an industrial electrolytic Cu powder that is united in a dendritic shape. Cu flakes of uniform size were obtained through high-energy ball milling. The Cu powder was flattened into thin flakes through physical processes such as collision, extrusion, and shear during the ball milling process[36]. Tert-butanol was used as the ball milling medium at a rotational speed of 250 rpm with a ball to material ratio of 15:1. The morphology and size distribution of the Cu flakes was observed at intervals of 2 h, 4 h, 6 h, 8 h and 10 h to determine the optimum ball milling time for the Cu powders. The Ti_3SiC_2 particles underwent refinement through high-speed ball milling for 1 h, using ethanol as a medium. The processed raw materials were dried in a vacuum freeze dryer for 24h.

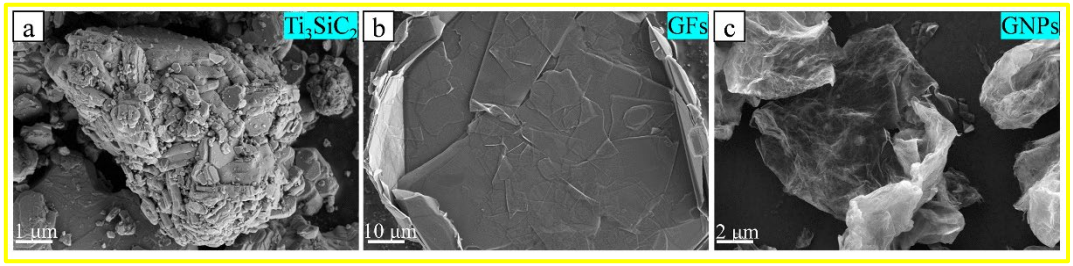

Fig. 1. Initial micromorphology of reinforced particles: (a) Ti_3SiC_2, (b) GFs, (c) GNPs.

2.2 Preparation of composites

The composites were designed and named as shown in Table 1. The composites

labeled as 0GNPs-S was created using clustered spherical Cu powders, while the composites labeled as 0GNPs-F, 0.5GNPs-F, 1.0GNPs-F, and 1.5GNPs-F were made using flake Cu powders with GNPs content of 0 wt %, 0 wt %, 0.5 wt %, 1.0 wt %, and 1.5 wt %. The GFs and Ti_3SiC_2 contents were maintained at 3.0 wt% and 10.0 wt %, respectively. The raw materials were added to the agate tank according to the predetermined composition and ball-milled for 1 h to obtain a homogeneously dispersed composite slurry. The slurry was then placed in a vacuum freeze dryer for 24 h to complete the drying process. The bimodal reinforced Cu/Ti_3SiC_2/C laminated-like composites were produced by placing the dried composite powder into a graphite mold and sintering it under vacuum hot pressing at a set pressure of 30 MPa, a sintering temperature of 950 ℃, and a holding time of 1 h. The finished sintered product was obtained following the experimental procedure shown in Fig. 2.

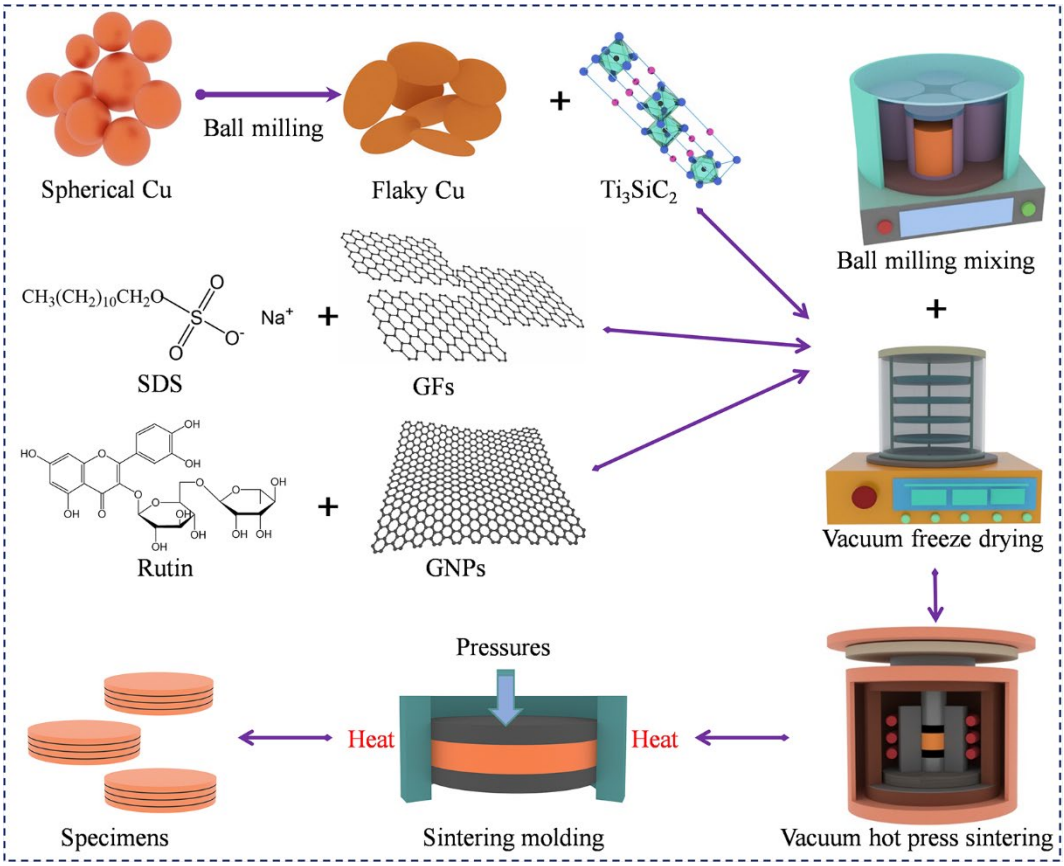

Fig. 2. Process flow of bimodal reinforced Cu/Ti_3SiC_2/C laminated-like composites

Table 1 Compositional design and nomenclature of composites.

Sample Designation	Cu (wt %)	Ti_3SiC_2 (wt %)	GFs (wt %)	GNPs (wt %)	Theory density (g/cm^3)
0GNPs-S	87.0 (Spherical)	10.0	3.0	0	7.51
0GNPs-F	87.0 (Flaky)	10.0	3.0	0	7.51
0.5GNPs-F	86.5 (Flaky)	10.0	3.0	0.5	7.38
1.0GNPs-F	86.0(Flaky)	10.0	3.0	1.0	7.25
1.5GNPs-F	85.5 (Flaky)	10.0	3.0	1.5	7.13

2.3 Characterization of composites

Fig. 3 shows samples of five bimodal reinforced Cu/Ti_3SiC_2/C laminated-like composites sintered and molded. The sample's density was determined to use Archimedes' principle, and its relative density was calculated by combining the theoretical density of the sample. Microhardness measurements were conducted using an HXD-100TM/LCD microhardness tester. The powders and samples were observed using a scanning electron microscope (SEM, ZEISS Sigma 300) and their elemental distribution was obtained using energy dispersive spectroscopy (EDS). The composites' physical phase composition was determined to use an X-ray diffractometer (XRD, Rigaku XRD-6100) and information such as crystal size and lattice strain was extracted from the XRD data using the William-Hall formula[37].

$$\beta = \frac{k\lambda}{D\cos\theta} + 4\varepsilon\tan\theta \qquad (1)$$

In this equation, D represents the grain size, λ represents the X-ray wavelength, ε represents the strain, β represents the diffraction peak half-height width (FWHM), k is a constant, and θ represents the diffraction peak position. The values for D and ε can be obtained by extracting the corresponding data and fitting it with Eq1.

The samples' microstructure and phase compositions were analyzed using transmission electron microscopy (TEM, FEI Talos F200X). The tensile strength and elongation of the samples was obtained using a microcomputer-controlled electronic universal testing machine (WDW-3100) at a strain rate of 0.5 mm/min. The EC was measured with a resistivity tester (FT-300A1). The laser thermal conductivity meter

(NETZSCH LFA467) was used to measure the thermal diffusion coefficient in the in-plane direction of the composites. The TC was then calculated using the provided equation[38]：

$$K = \alpha \cdot \rho \cdot \sum f_i C_p^i \qquad (2)$$

The TC, K, is measured in $W \cdot m^{-1} \cdot K^{-1}$. The thermal diffusion coefficient, α, is measured in m^2/s. The density, ρ, is measured in kg/m^3. The specific heat capacity of phase i, C_p^i, is measured in J/(kg·k), and f_i represents the volume fraction of phase i.

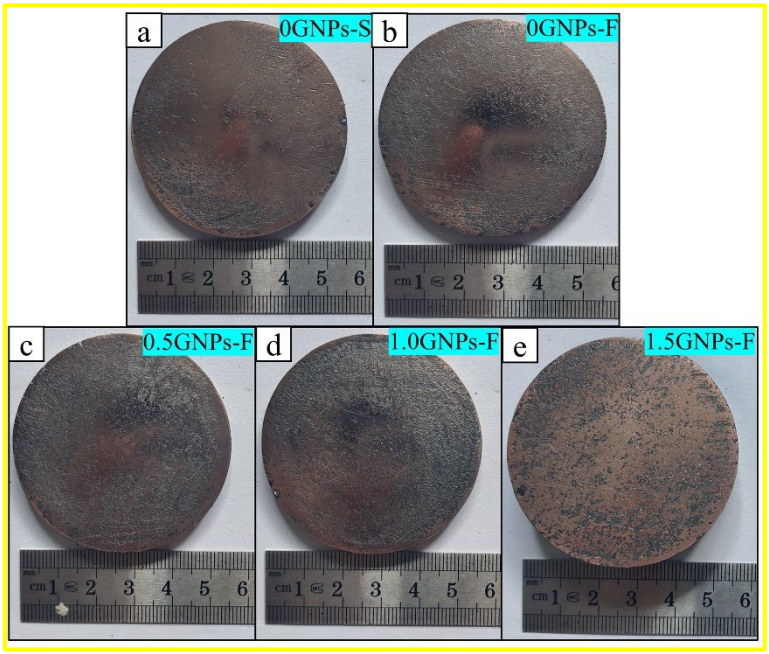

Fig. 3. Macroscopic images of composites samples at millimeter scale: (a) 0GNPs-S, (b) 0GNPs-F, (c) 0.5GNPs-F, (d) 1.0GNPs-F, (e) 1.5GNPs-F.

3. Analysis and discussion

3.1. Microstructure of composites

3.1.1 Cu flake and composite powder microstructure

High-energy ball milling can activate the powder, generate new grain boundaries and phase boundaries, and shape the powder into new forms[39]. Regulating the ball milling parameters can produce Cu powder with good plasticity and an ideal distribution of flake size. This flake Cu powder serves as the basis for preparing laminated-like Cu matrix composites[35]. Tert-butanol is often used as the ball milling medium to moderate temperature increase and increase powder viscosity and fluidity. The raw Cu powder used in this study was grown from ellipsoidal Cu particle clusters, which is a beneficial structure for soldering between particles and improving flake shaping efficiency, as shown in Fig. 4a. As demonstrated in Fig. 4b and 4c, the Cu powder clusters were gradually compressed and thinned through collision extrusion and shear. Small particles fill the gaps between particles, and broken agglomerates begin to adhere and gather together. After 6 h of ball milling (Fig. 4d), the Cu powders began to form uniform flakes. However, there was still a significant adhesion between the particles, and the assembly of flakes was incomplete. After 8 h of ball milling (Fig. 4e), the flake Cu powders became thinner, the adhesion between the particles reduced, and the assembly between the flakes improved. However, when the ball milling time was extended to 10 h (Fig. 4f), the frequent collisions and extrusions between the flakes and balls caused a sharp increase in the surface energy of the Cu flakes. This increase exceeded the tolerance limit of the flake Cu powders, causing it to break down into smaller particles. In order to further investigate the size change of Cu powders in ball milling and the optimal ball milling time, the size distribution of Cu flakes in ball milling for 4-10 h was counted in this paper. Fig 4c$_1$-f$_1$

shows that the flake diameter of Cu powder gradually increased, and the flake rate increased with longer ball milling time. After 8 h of ball milling, the particle size distribution is normal, with the majority of particles concentrated in the 45-60 μm range, which is optimal for flake assembly during sintering.

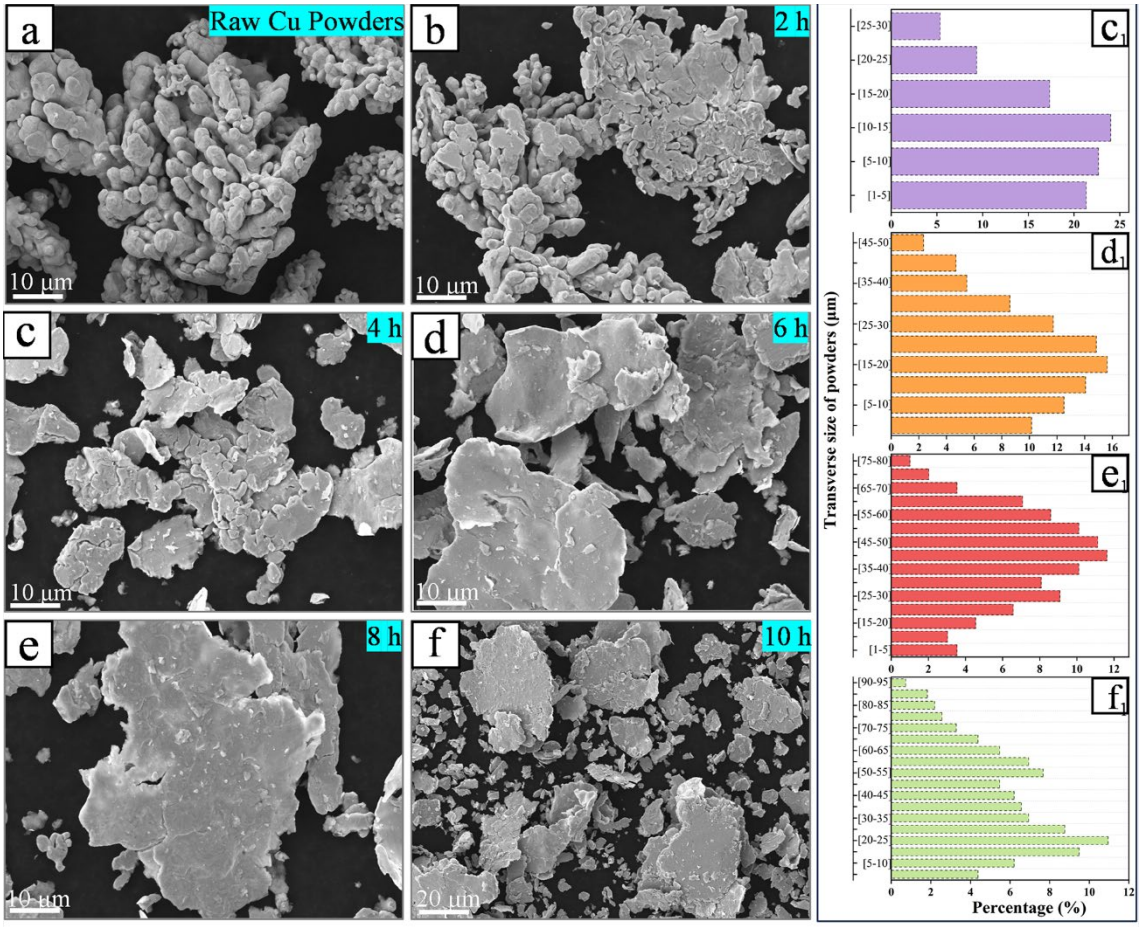

Fig. 4. Microscopic morphology of Cu powder after ball milling: (a) original Cu powder, (b) 2 h, (c) 4 h, (d) 6 h, (e) 8 h, (f) 10 h; Transverse dimensional statistics of ball milled powder: (c_1) 4 h, (d_1) 6 h, (e_1) 8 h, (f_1) 10 h.

The Cu flakes were mixed with three proportionally added reinforcing phase particles in an agate vessel for 1 h. The microscopic morphology of the composite powder is shown in Fig. 5a. Some of the small-sized GNPs were embedded in the surface of Cu

flakes under the action of ball milling, and Ti_3SiC_2 showed agglomerated spherical particles. The EDS results of the composite powders are shown in Fig. 5(a_1-a_4), and the components are well distributed. On the one hand, a shorter period of ball milling increases the chance of contact between particles and helps to ensure uniform dispersion of the reinforcing phase in the matrix. On the other hand, it can prevent the copper flakes from breaking and too many defects on the surface of GFs and GNPs.

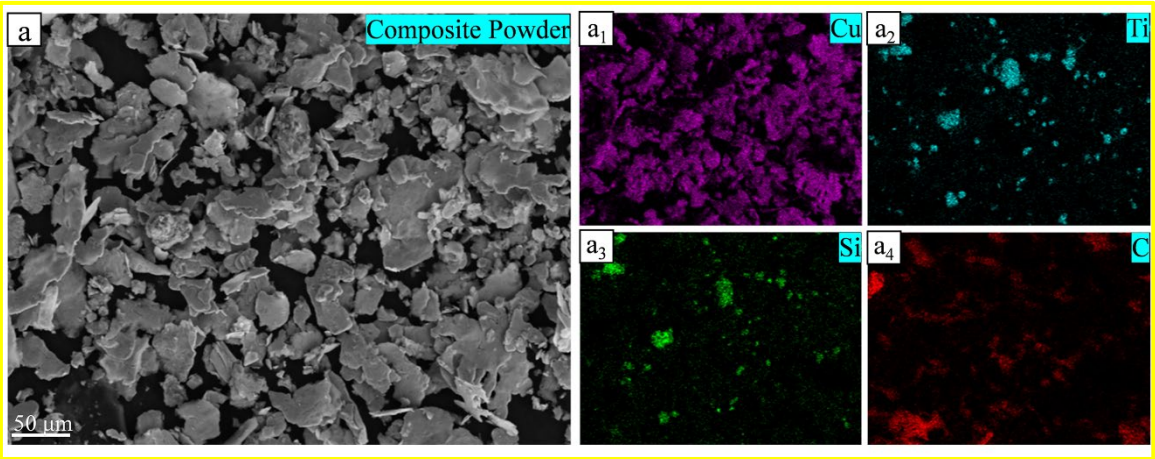

Fig. 5. (a) Microscopic morphology of the composite powder after ball milling and mixing for 1h, (a_1-a_4) the distribution of Cu, Ti, Si and C elements, respectively.

3.1.2 Phase composition

Fig. 6a displays the XRD spectra of the laminated-like composites. At high temperatures, Ti_3SiC_2 undergoes thermal decomposition and reacts with Cu to form the hard and brittle phase TiC and the solid solution phase Cu_9Si [16, 40]. The detected substances were present in all five composites with varying GNPs contents, indicating that the reactions of Cu and Ti_3SiC_2 were not influenced by GNPs. Fig. 6b displays the grain size and lattice strain of the laminated-like composites. The relationship between

grain size and lattice strain for GNPs content ≤ 1.0 wt% follows the typical response of the Williamson relationship[20]. The decrease in grain size can be attributed to two main reasons. The significant reduction in size is due to sintering recrystallization refinement after plastic deformation. High-energy ball milling causes local stress and strain concentration, as well as work-hardening of the Cu particles. This provides morphogenetic energy to drive recrystallization and further grain refinement during the sintering process[35]. Furthermore, the introduction of GNPs can also contribute to the process. GNPs with a large surface area can provide effective sites for grain nucleation, promoting the nucleation of new phases, as well as pinning grain boundaries, which slows down the migration of grain boundaries and inhibits grain growth[37]. Prolonged ball milling increases the residual compressive stress after sintering of Cu particles, leading to an increase in lattice strain. Lattice strain is further increased due to the interaction of lattice mismatch and thermal mismatch between GNPs and Cu[39]. Grain size and lattice strain are positively proportional when the content of GNPs > 1.0 wt%. At this point, GNPs exceeding the limiting value leads to an increase in the agglomeration region, a decrease in the effective nucleation sites, and a gradual failure of the ability to inhibit grain boundary migration, which in turn leads to grain coarsening. Nevertheless, the grain size of the bimodal laminated-like composites was significantly reduced compared to that of the conventional structural composites. This confirms the beneficial effect of FPM and GNPs in refining the grains.

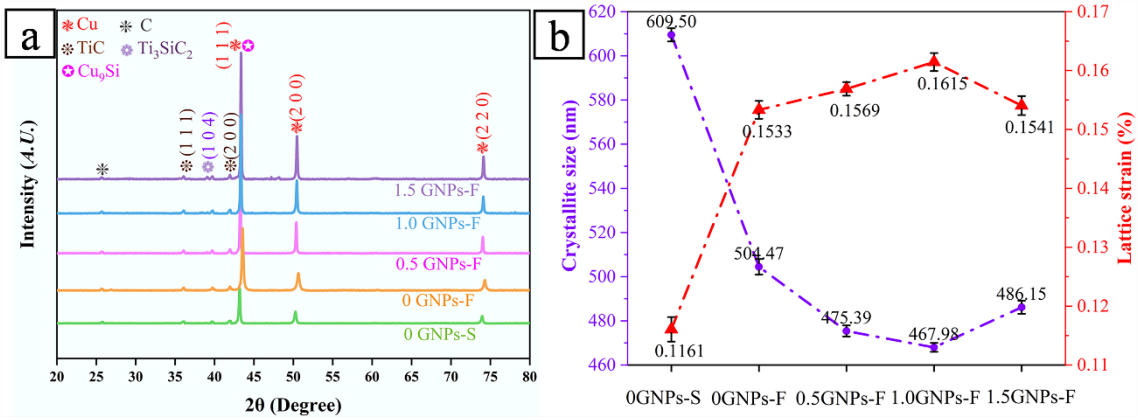

Fig. 6. (a)XRD pattern of the bimodal reinforced Cu/Ti_3SiC_2/C laminated-like composites, (b) Grain size and lattice strain in bimodal reinforced Cu/Ti_3SiC_2/C laminated-like composites.

3.1.3 Cross-sectional microstructure

Fig. 7a shows that the matrix of 0GNPs-S composites is spherical Cu, resulting in irregular phase distribution. The light gray region represents Cu matrix, the dark gray agglomerated region represents Ti_3SiC_2, and the black particles without uniform orientation distribution represent GFs. The interfacial bonding between Ti_3SiC_2 and Cu is strong due to thermal decomposition and interfacial reaction[40]. Regarding the composites of 0GNPs-F with Cu flakes as the matrix, the reinforcing agent GFs is distributed between the Cu flakes and aligned along the planar direction. This result in an obvious laminated-like arrangement with a single-peak laminated-like structure, as shown in Fig. 7b. The flake Cu, with its excellent aspect ratio, serves as the basis for assembling the laminated-like structure. During the sintering process, the reinforcing particles and Cu flake self-assembled under gravity. High temperature and pressure caused bonding

and diffusion between the Cu flakes, resulting in a laminated-like structure resembling a pearl shell[41]. As shown in Fig. 7c,d, the incorporation of GNPs makes the laminated-like phase more pronounced and the continuity is significantly enhanced compared to the unimodal laminated-like structure. Due to the different sizes of GFs and GNPs, their bimodal enhancement properties are obvious. The incorporation of large-sized GFs provides some ductility and energy absorption, which enhances the overall toughness of the material. In contrast, the smaller sized GNPs exhibit size and bonding effects that increase strength and hardness[42]. The stacking or alternating arrangement of larger-sized GFs and smaller-sized GNPs is an important component of the laminated-like structure, which is therefore defined as a bimodal laminated-like structure.

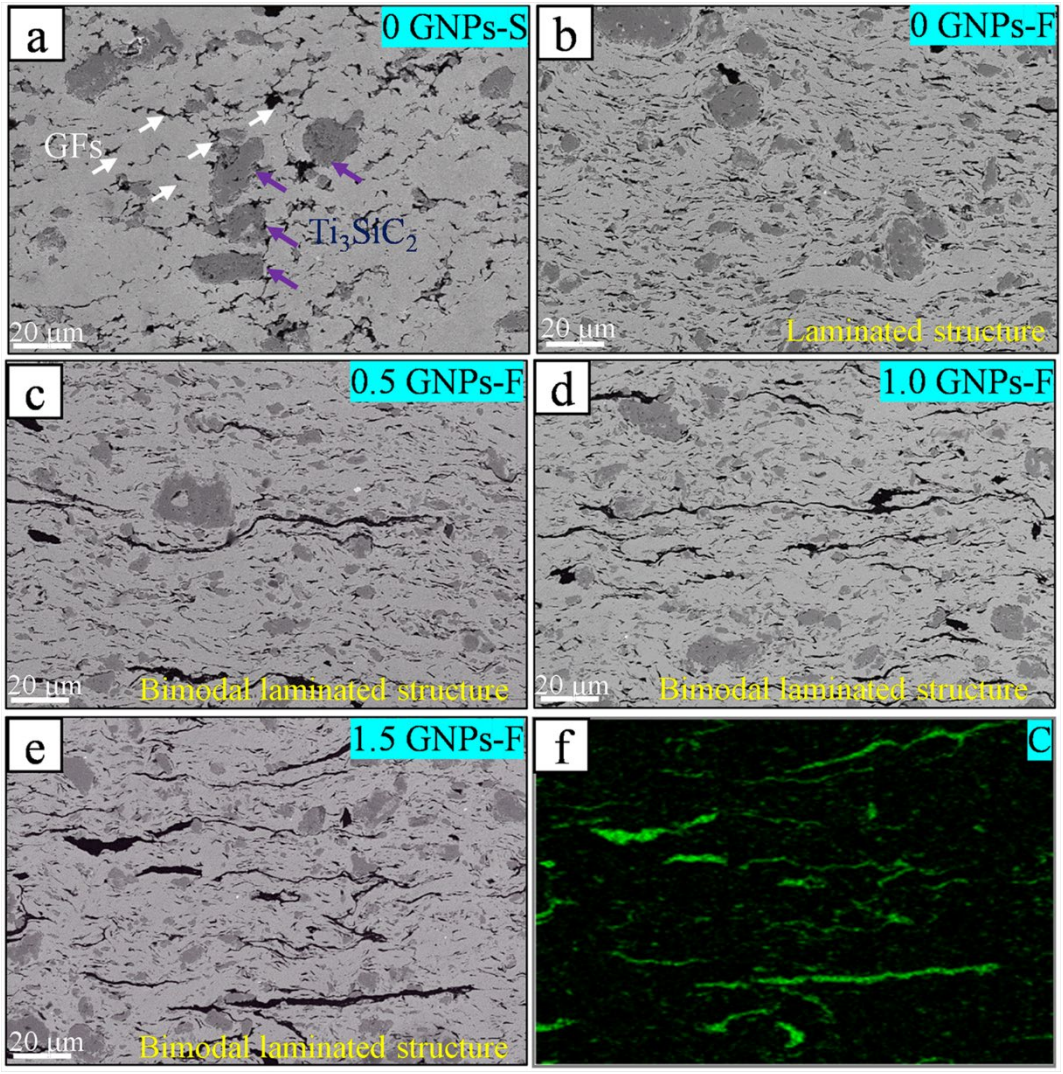

Fig. 7. Cross-sectional microstructures of bimodal reinforced Cu/Ti_3SiC_2/C laminated-like composites: (a) 0GNPs-S, (b) 0GNPs-F, (c) 0.5GNPs-F, (d) 1.0GNPs-F, (e) 1.5GNPs-F, (f) distribution of element C.

An alignment model was used to statistically characterize the orientation law of self-assembled flake powder particles, GFs and GNPs under sintering pressure to understand this type of assembly[43, 44]:

$$< cos^2\ \theta >= \frac{\int \rho(\theta) cos^2\ \theta sin\ \theta d\theta}{\int \rho(\theta) sin\ \theta d\theta} \quad (3)$$

$$\rho(\theta) = A_1 e^{\left(\frac{-\theta}{t_1}\right)} + y_0 \quad (4)$$

The θ between the two-dimensional plane direction of the reinforcing phase (GNPs and GFs) and the in-plane direction of the composites was statistically obtained from the microstructure images of the composites ($0° \leq \theta \leq 90°$). Reinforcing phase GFs of composites 0GNPs-S is not included in the statistics because they are completely randomly distributed. Statistical function ρ(θ) describes the distribution of the reinforcing particles (GFs, GNPs) in the composites. It is an oriented distribution represented by the fitting parameters A_1, t_1, and y_0. $\langle\cos^2\theta\rangle$ describes the alignment orientation of the reinforcement in the composites, as shown in Fig. 8. The value of $\langle\cos^2\theta\rangle$indicates the degree of alignment of the 2D planar direction of the reinforcing particles with the in-plane direction of the composites. A value closer to 1 indicates a more perfect parallel alignment, while a value closer to 0 indicates a skew towards the through-plane direction. The higher the probability that the reinforcing particles are randomly aligned in orientation, the closer $\langle\cos^2\theta\rangle$ is to 1/3[45].

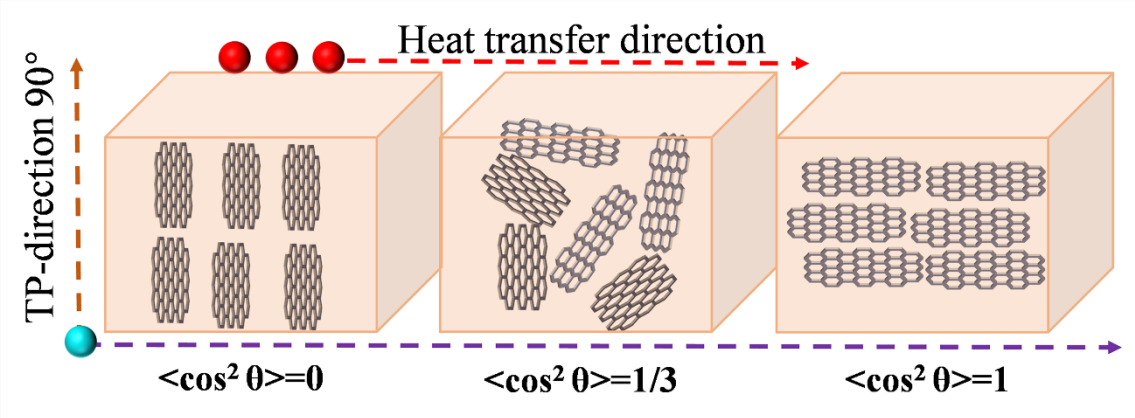

Fig. 8. Schematic of alignment of bimodal reinforced Cu/Ti_3SiC_2/C laminated-like composites.

Fig. 9 shows the statistics and alignment fitting results of $\langle\cos^2\theta\rangle$ values of GFs

and GNPs in the laminated-like composites. The $\langle\cos^2\theta\rangle$ of GFs in the 0GNPs-F composites is 0.90, indicating relatively good alignment of the GFs particles in the in-plane direction. This is due to the compressive stresses in the hot-pressing process promoting the rotation of 2D-reinforced particles in the in-plane direction. However, there is a difference in the $\langle\cos^2\theta\rangle$ values of GFs and GNPs in the same composites (4.1-9.6%). This difference is due to the variation in aspect ratios of the two reinforcing phases ($A_{GFs} < A_{GNPs}$, where A is the aspect ratio), the difference in resistance to particle rotation under compressive stress, and the difference in the magnitude of rotation in the in-plane direction[46]. Furthermore, as the content of GNPs increases, the volume of GFs and GNPs decreases, and the $\langle\cos^2\theta\rangle$ value also decreases, indicating that their alignment orientation begins to deviate from the in-plane direction. This is consistent with the observed microstructural results. Due to van der Waals forces, some GNPs particles adhere between the flakes of GFs with larger particle sizes, preventing the GFs from rotating in the in-plane direction and leading to the deterioration of their arrangement[22]. Meanwhile, compressive stress also inhibits the tendency of GFs and GNPs to agglomerate towards the center. GFs and GNPs extend in the planar direction with the flow of semi-molten Cu particles, leading to the formation of a laminated-like phase with excellent continuity. These findings confirm the high efficiency of flake powder metallurgy and hot press sintering in preparing laminated-like composites.

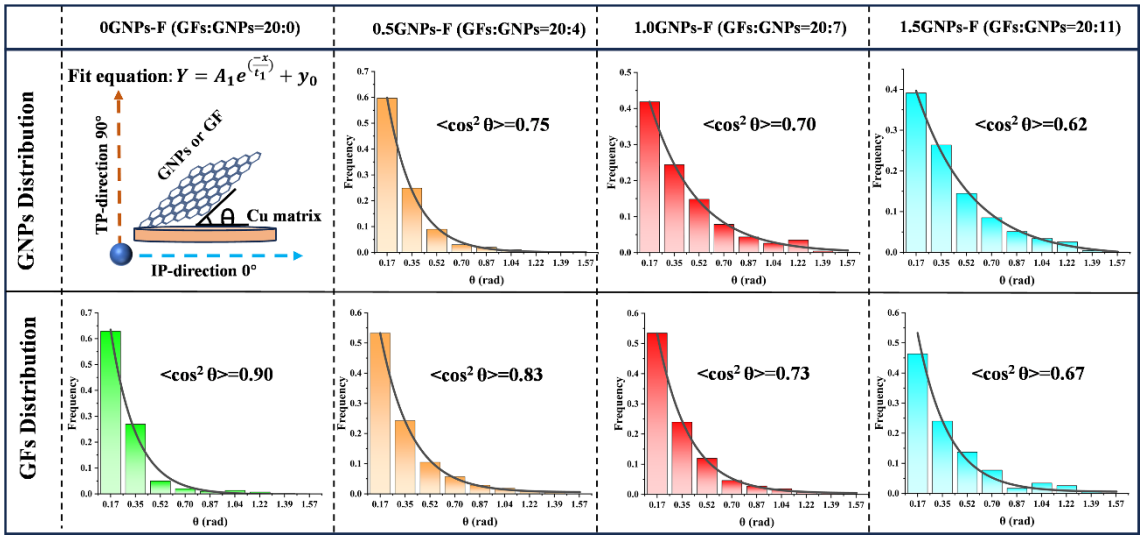

Fig. 9. Statistics and alignment fitting of theta values of GFs and GNPs in bimodal reinforced Cu/Ti_3SiC_2/C laminated-like composites.

3.1.4 Microregion interface structure

Fig. 10 displays TEM images of bimodal reinforced Cu/Ti_3SiC_2/C laminated-like composites. The interface between Cu and Ti_3SiC_2 is well-defined with obvious morphological differences. However, under high resolution, the interface appears blurred with a distinct transition layer. This indicates that the interaction between Cu and Ti_3SiC_2 generates new phases at the interface, enhancing the thermally stable bonding of the two phases. Fig. 10d displays the new phase TiC as alternating light and dark stripes with a larger layer spacing than that of Ti_3SiC_2. The formation of these laminated stripes is due to elemental diffusion and in-situ reaction between Cu and Ti_3SiC_2. Fig. 10h illustrates that Cu has a high diffusivity and infiltrates the interstitial space of Ti_3SiC_2 particles at high temperatures. This infiltration induces thermal decomposition of Ti_3SiC_2 and weakens Ti-Si bonding, resulting in Si de-embedding. Free Si then penetrates the matrix

to form solid solution Cu_9Si, resulting in a similar elemental distribution of Si and Cu near the interface. The new phase TiC is generated in situ through thermal decomposition, while the good wettability of TiC and Cu facilitates further Cu diffusion[47]. Cu and TiC that had infiltrated was spaced to form laminated streaks, which is consistent with the results observed in the EDS energy spectrum (Fig. 10b). To mitigate the thermal stress caused by the difference in thermal expansion coefficients between the two phases of TiC-Cu, dislocations need to be introduced at or near the interface, resulting in a large number of dislocations accumulating at the interface of the two phases of TiC-Cu[40]. As a result, the interfacial reaction between Cu and Ti_3SiC_2 enables the two phases to form a strong, thermally stable metallurgical bond, which enhances the wettability of the system.

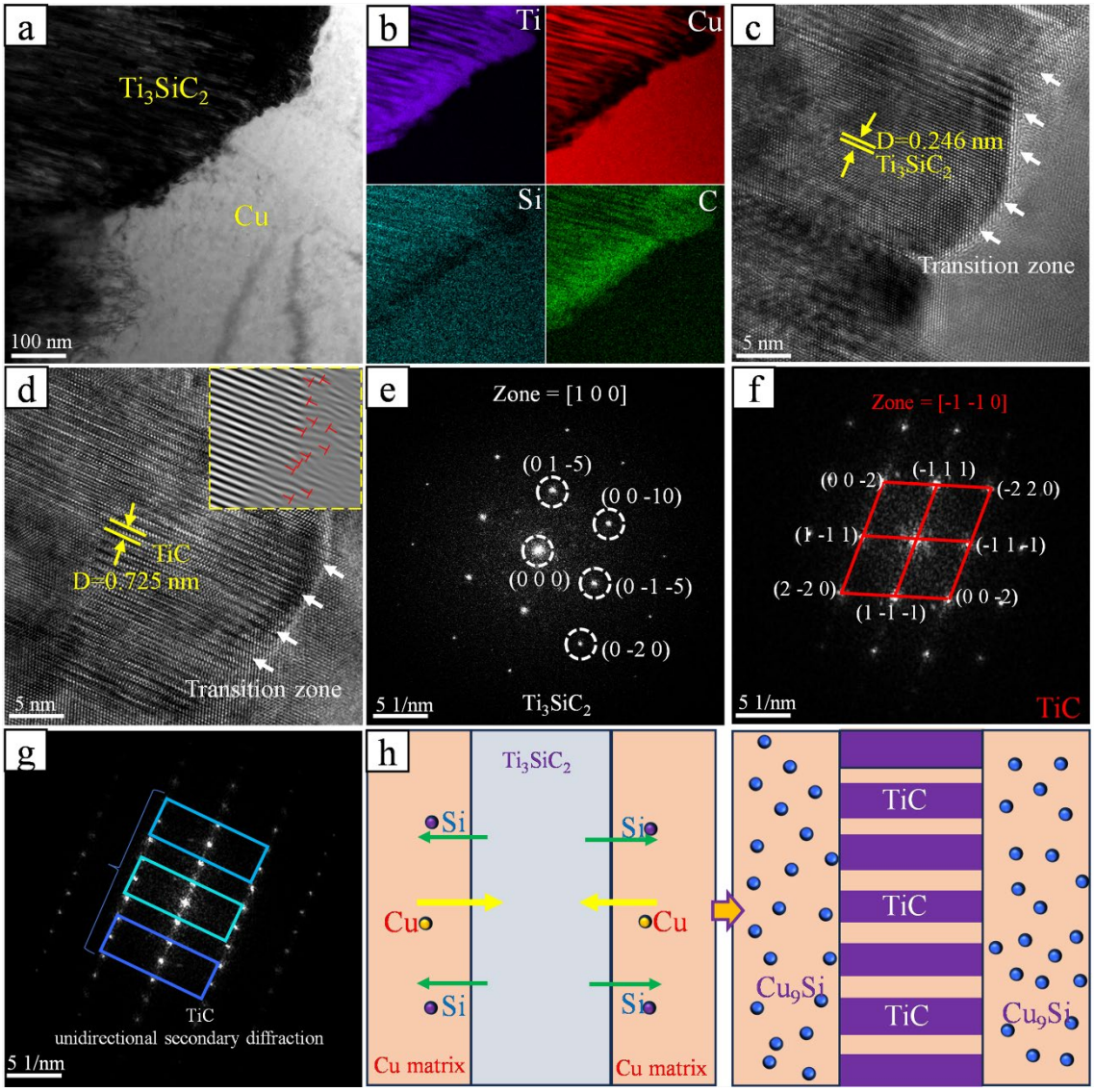

Fig. 10. TEM images of bimodal reinforced Cu/Ti_3SiC_2/C laminated-like composites: (a, b) bright field images and EDS mapping images, (c) high-resolution image of the interface of Cu-Ti_3SiC_2, (d) high-resolution image of the interface of Cu-TiC, (e) diffraction pattern of Ti_3SiC_2, (f, g) diffraction pattern and secondary diffraction pattern of TiC, (h) schematic of the interfacial reaction of Cu-Ti_3SiC_2

Fig. 11 shows that the alignment orientation of GNPs at the nanoscale remains close to and parallel with the in-plane orientation. Interface between GNPs and Cu is well-

defined, and even in high-resolution images, there is still a clear boundary without any gaps. This is because the weak van der Waals forces drive the interaction force at the interface of the two phases, which can only promote the physical attachment of the two phases to form mechanical bonding[48]. The interfacial bonding of the two phases is strengthened by high-temperature plastic deformation and shear strain, which enhances the mechanical bonding. Ti_3SiC_2 is also present in the form of small particles near the interface of GNPs and Cu. Due to elemental diffusion, Ti_3SiC_2 at the interface effectively improves the bonding strength of GNPs and Cu (Fig. 11b). Meanwhile, the energy generated during the ball milling process results in the high surface energy of GNPs. To reduce this surface energy, atomic reorganization is typically employed to form wrinkles on the surface or produce the edge effect [49], as shown in Fig. 11e. This folding increases the inherent roughness of the GNPs and enhances the bond strength with Cu. In conclusion, Cu is tightly bound to the reinforcing phases GNPs and Ti_3SiC_2 in different bonding forms, which effectively reduces the presence of interfacial porosity, thus inhibiting crack nucleation and decreasing phonon scattering to some extent.

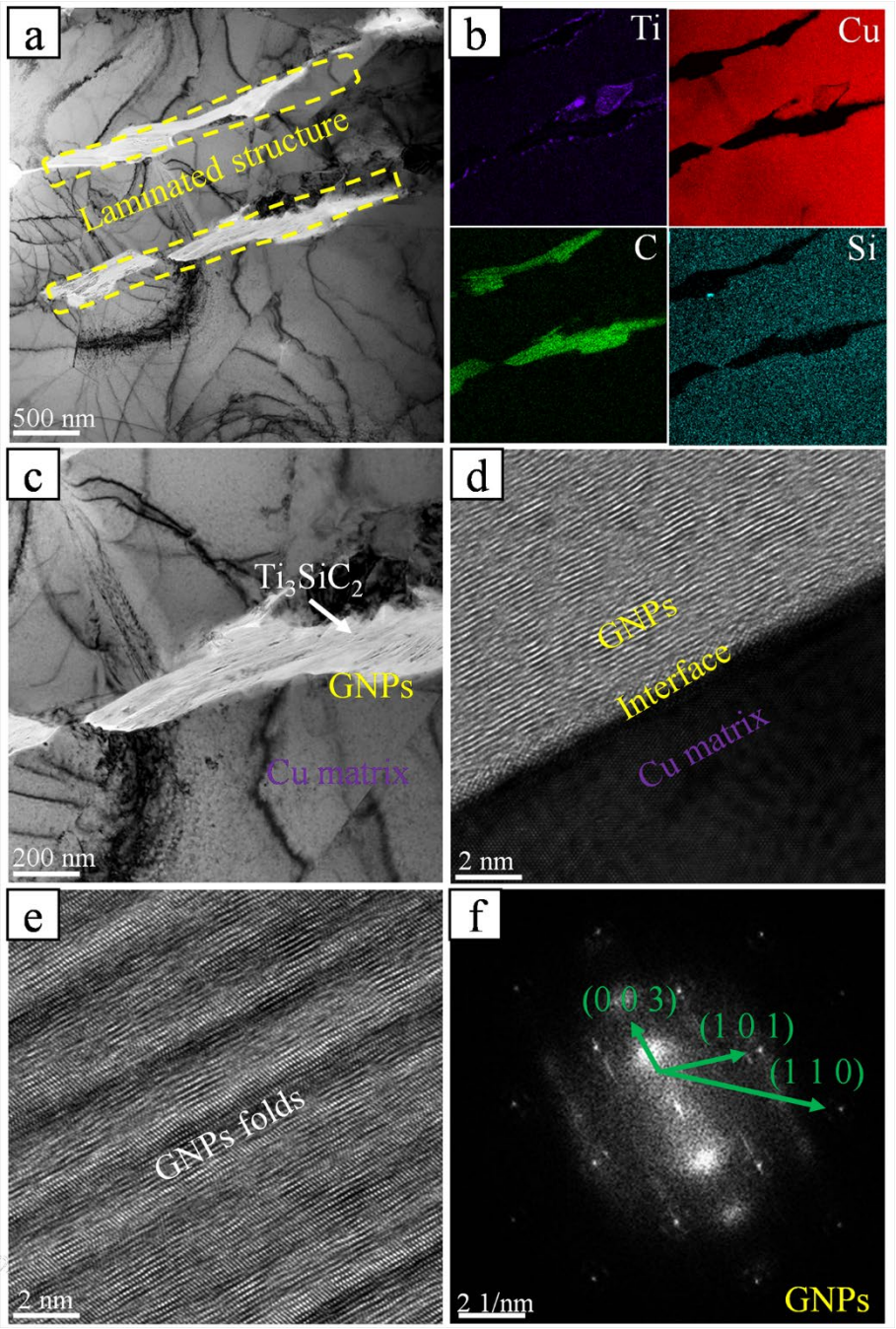

Fig. 11. TEM images of bimodal reinforced Cu/Ti_3SiC_2/C laminated-like composites; (a) laminated-like structure, (b) EDS mapping images of Fig. 11a, (c) microstructure, (d) high-resolution image of the interface of Cu-GNPs, (d)GNPs folds, (f) diffraction pattern of GNPs.

3.2. Mechanical properties

Fig. 12a shows the relative density and micro-hardness of Cu/Ti_3SiC_2/C bimodal reinforced laminated-like composites. The relative densities of the composites, measured by the Archimedean drainage method, are all above 96% and within 0.27 standard error. The mechanical properties of the composites are particularly dependent on a good densification, characterized by a homogeneous internal organization and a low level of defects[50]. Optimal densification allows for efficient load transfer and maximizes the contribution of reinforcing fibers to composite strength[51]. Due to the tendency of GFs and GNPs to resist wetting at the Cu-C interface, it will lead to a difficulty in achieving adequate bonding between the two phases and will form micro-pores during the sintering process, ultimately hindering the densification process and internal organization[5]. The micro-hardness of composites is influenced by various factors, such as the design of the laminated-like structure, which impacts the spatial orientation and distribution of the reinforcing phases. The laminated-like structure is well-designed to enhance packing density and tissue hardening. Moderate doping of GNPs strengthens the local resistance of composites to external forces due to the unique mechanical properties of GNPs[52]. However, the effect of GNPs on micro-hardness is dependent on the quantity introduced. If the amount of GNPs exceeds a certain threshold, it can lead to a decrease in material homogeneity due to agglomeration and an increase in porosity, resulting in reduced composite hardness. Both Ti_3SiC_2 and its reaction product, TiC, are harder than the matrix and exhibit high-quality bonding with the matrix Cu, which facilitates the compaction of

composites. Consequently, the uniform distribution of Ti_3SiC_2 in the matrix can markedly enhance the hardness of the composites. Furthermore, the ball milling process used in manufacturing introduces defects in the GNPs, which can compromise the integrity and hardness of the composites[53].

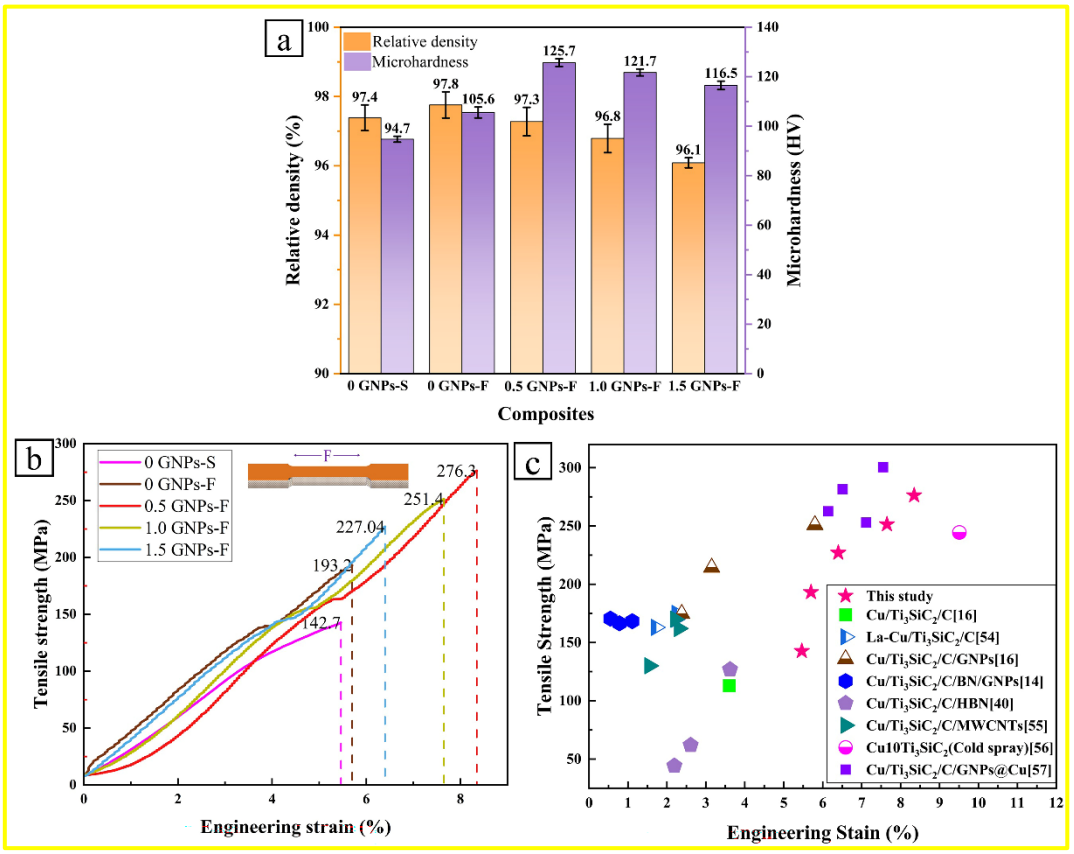

Fig. 12. Mechanical properties of bimodal reinforced $Cu/Ti_3SiC_2/C$ laminated-like composites:(a) microhardness and relative density, (c) Comparison of tensile strength with other similar composites[14, 16, 40, 54-57].

Fig. 12b shows the results of the tensile tests conducted on bimodal reinforced $Cu/Ti_3SiC_2/C$ laminated-like composites in the direction parallel to the laminated-like structure. The 0GNPs-S composites have a conventional structure and the 0GNPs-F composites have a single-peak laminated-like structure, the latter having an increased

tensile strength of 50.5 MPa. The composites with the introduction of 0.5 wt% GNPs (0.5GNPs-F) exhibit a bimodal laminated-like structure and an enhanced tensile strength of 83.1 MPa compared to the composite without GNPs (0GNPs-F). Laminated-like structure and GNPs are the main contributors to the enhancement of tensile strength in the composites. However, increasing the content of GNPs leads to a decrease in tensile strength. This may be due to the excessive content of GNPs and agglomeration, which can lead to the generation of defects such as micro-pores near the Cu-C interface. These defects negatively affect the strength enhancement of the composites, offsetting part of the positive effect of the inherent strength of GNPs. Nevertheless, the composites designed in this study performed well in terms of tensile strength and elongation compared to other similar composites, as shown in Fig. 12c. This may be due to the unique bimodal laminated-like structure. Therefore, the mechanism of strengthening and toughening of the composites will be investigated in conjunction with the fracture behavior of the composites.

The morphological differences in the tensile fracture of composites with three different structures were analyzed and compared to investigate the strengthening mechanism of the laminated-like structure and GNPs on the composite strength. Fig. 13a,a_1 shows that the fracture surface of 0GNPs-S composites with conventional structure has irregular distribution of each phase, and exhibits dimple and cavitation phenomena, presenting a typical honeycomb shape. Fracture morphology of the 0GNPs-F composites changed significantly due to the construction of a single-peak laminated-like structure.

GFs were interspersed between the Cu flakes in a highly oriented arrangement, as shown in Fig. 13b,b$_1$. Fracture laminated-like structure of the 0.5GNPs-F composites was more clearly defined, presenting a bimodal laminated-like structure with the two phases of the GFs and the GNPs occupying the positions between the Cu flakes alternately, as shown in Fig. 13c,c$_1$. The number of dimples is reduced, indicating that the load of the composites primarily relies on the transfer of interlayer GNPs. This was accomplished through the pulling out or breaking of GNPs.

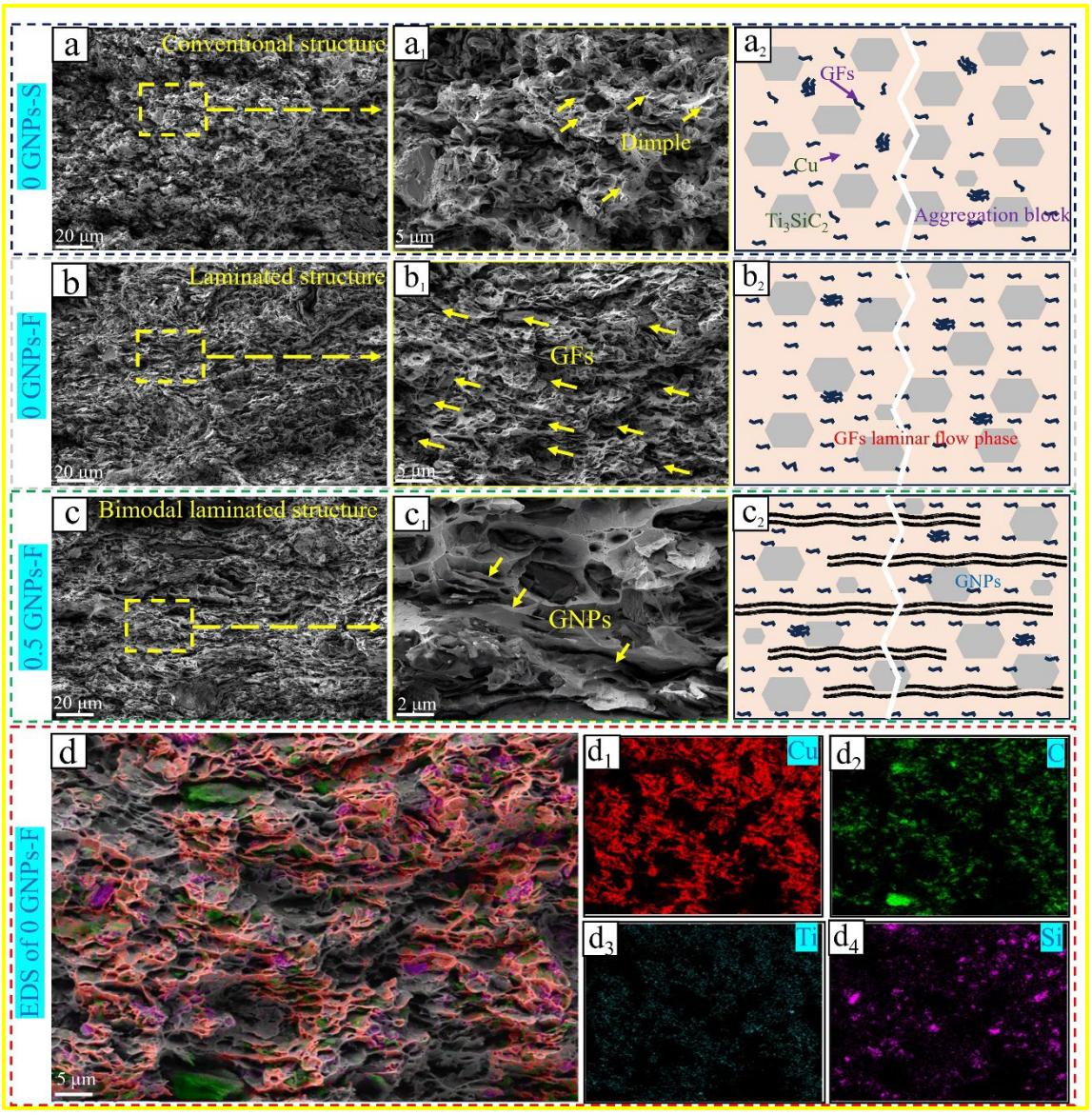

Fig. 13. Tensile fracture morphology and fracture schematics of bimodal reinforced Cu/Ti_3SiC_2/C laminated-like composites:(a-a_2) 0GNPs-S, (b-b_2) 0GNPs-F, (c-c_2) 0.5GNPs-F, (d-d_4) EDS image of 0GNPs-F.

As demonstrated in Fig. 13a_2-c_2, composites display varying strengthening mechanisms and failure forms due to their distinct structures or strengthening phases. In the case of the conventional structure, the aggregated GFs cause voids to form on the weakly bonded interfaces of Cu particles. Under tensile loading, these micropores are located in the stress concentration region, leading to crack initiation and extension. Cracks propagate along the interfaces between weakly bonded particles, causing particle de-embedding and fracture within the crystal. This ultimately results in a dimple on the fracture surface. The unimodal laminated-like structure features a highly dispersed arrangement of GFs, which forms a large number of Cu-C micro-interfaces. As shown in Figs. 13d-d_4, the results of tensile fracture of the composites shown in the EDS images indicate that the distributions of matrix and reinforcement phases are complementary to each other. This uniformly distributed interfacial fetch serves to inhibit dislocation motion, thus enhancing the strength of the composites. In addition, the thermal mismatch between Cu and GFs can cause a concentration of interlaminar internal stresses when the composites are loaded. However, the laminated-like structure not only withstands these internal stresses but also efficiently disperses them, reducing the possibility of strain localization and subsequent failures[15]. The laminated-like structure, which is bimodal, introduces GNPs as a high-strength phase. Under tensile load, the Cu matrix deforms and

the GNPs act as a bridge for load transfer between matrix flakes. This improves the load distribution, inhibits crack initiation, and allows for crack tip bridging[23]. When the applied load surpasses the strength limit of the Cu matrix, cracks expand. The process of pulling some GNPs out of the matrix requires energy, which dissipates part of the load, contributing to the material's toughness. Non-coherent interfaces can impede the transfer of load from the matrix to the GNPs[58]. Therefore, a strong interfacial bond between Cu and GNPs is crucial for efficient load transfer and energy dissipation. These factors are essential for enhancing material toughness and preventing crack propagation.

The strengthening of composites' performance often involves multiple mechanisms, including load transfer in laminated-like structures and GNPs. Additionally, changes in grain size play a crucial role. XRD correlation results demonstrate a significant reduction in composite grain size, indicating an increase in the number of grain boundaries. A high density of grain boundaries obstructs dislocation movement, leading to dislocation buildup within the boundaries. This enhances the interaction between dislocations and grain boundaries, resulting in a stronger material[58]. For GNPs content of 0.5 wt% or less, the change in grain size is inversely proportional to the changes in hardness and tensile strength, consistent with the Hall-Petch relationship[59]. The relationship mentioned above does not apply when the content of GNPs is greater than 0.5 wt%. This indicates that the share of contribution of fine-grain strengthening and load transfer is largely determined by the content and distribution of GNPs. GNPs with lower content (around 0.5 wt%) can perform the roles of both fine-grain strengthening and load transfer,

while GNPs with higher content (≥1.0 wt%) restrict the contribution of both mechanisms.

3.3. Thermal conductivity

Theoretical TC of bimodal reinforced Cu/Ti_3SiC_2/C composites was modeled using the effective medium approximation (EMA) [60]:

$$K_c = V_1K_1 + V_2K_2 \tag{5}$$

$$K_i = K_m\{\frac{2 + V_i\beta_{//}(1 + (\cos^2\ \theta))}{2 - V_i\beta_{\perp}(1 - (\cos^2\ \theta))}\} \tag{6}$$

With

$$\beta_{//} = \frac{L_i}{K_m} - 1, \beta_{\perp} = 1 - \frac{K_m(R_{Ki}L_i/t_i + 1)}{L_i} \tag{7}$$

Where K_c represents the theoretical TC of the composites in-plane, V_i is the volume fraction of reinforcing particles i, K_i is the TC of reinforcing phase i synergize with the matrix in the in-plane direction, and K_m is the TC of the Cu10Ti_3SiC_2 matrix. The thickness of the reinforcing phase i are represented by t_i, where t_{GFs}=10^{-5}m and t_{GNPs}=$2\cdot10^{-8}$m. L_i represents the theoretical TC of reinforcing phase i in the in-plane direction, where L_{GFs}=1200 $W\cdot m^{-1}\cdot K^{-1}$ and L_{GNPs}=5000 $W\cdot m^{-1}\cdot K^{-1}$. The R_K (Kapitza thermal resistance) of the Cu-GFs and Cu-GNPs are $3.58\cdot10^{-8}$ m^2/kW and $1.0\cdot10^{-9}$ m^2/kW, Ref[61].

The layered-parallel method was utilized to predict the TC in the plane direction of anisotropic reinforced-phase composites based on the above model. This method examines factors such as reinforced-phase volume fraction, alignment, and interfacial thermal resistance, and compares the

theoretical values with the measured ones (Fig. 14). The results indicate that the TC of the 0GNPs-F specimen with a laminated-like structure is significantly higher than that of the 0GNPs-S specimen, even when the composition ratio of the composites is the same. This suggests that the laminated-like structure effectively improves the TC of the composites. The TC of both the composites, as measured and theoretically calculated, showed an increasing trend with the increase in GNPs content. The actual TC of the composites was the highest at 254.7 $W \cdot m^{-1} \cdot K^{-1}$ when the GNPs content was 1.5 wt%. This increase was attributed to the intrinsic ultra-high TC of GNPs. However, the measured TC values of the composites were found to be significantly lower than the theoretical values. On the one hand, the theoretical model employed in this study is predicated on calculations conducted under ideal conditions, wherein it is assumed that the material is devoid of defects and that full contact is evident at all interfaces. Secondly, numerous microscopic factors during the molding and characterization of composites may contribute to increased deviation, including interfacial thermal resistance, porosity, and the distribution and orientation of the nano-reinforced materials.

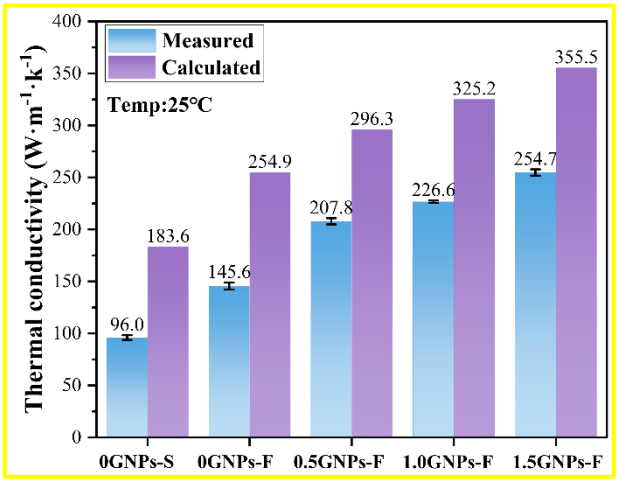

Fig. 14. Measured and theoretical TC of bimodal reinforced Cu/Ti_3SiC_2/C laminated-like composites.

Fig. 15 illustrates the various forms of heat transfer in bimodal reinforced Cu/Ti_3SiC_2/C laminated-like composites. These forms can be distinguished based on the size and distribution of the reinforcing phases, as well as the interactions between heat carriers, such as electrons and phonons[5]. In the reinforced phase-poor region of composites, heat transfer behavior is similar to that of pure metals. Heat transfer is mainly carried out through the free electron-directed motions within Cu with the temperature gradient. In matrix-dominated regions, heat transfer efficiency is often limited by factors such as matrix structural defects and thermal barriers. These barriers include pores, grain boundaries, and the low-conductivity phase Ti_3SiC_2, which scatters electrons and impedes heat flow[26]. In contrast, the enhanced phases GFs and GNPs have excellent TC due to phonons and 2D electron gases. When they form a continuous network, known as a percolation

network, in the matrix, they provide direct heat flow paths around the matrix, creating phonon TC paths[62]. The transfer of heat through the phonon conduction path is highly efficient, but it is heavily influenced by the content and distribution orientation of GFs and GNPs. This effect on heat transfer is only noticeable when their concentration reaches the percolation threshold. This threshold is the critical concentration of GFs and GNPs required to form a continuous heat conduction network throughout the matrix[63]. Thus, the TC of bimodal reinforced Cu/Ti_3SiC_2/C composites increases with the elevated content of GNPs. However, the increment is limited, which is in line with the experimental results. When the matrix Cu is alternately distributed with GFs and GNPs, the efficiency of heat transfer also depends on the quality of the interfacial bond between the two phases. The absorption or emission of phonons by electrons during lattice motion is known as the thermal energy carrier coupling effect, which can improve the energy transfer efficiency[22]. However, weaker interfacial adhesion energy tends to reduce the effective heat transfer at the interfaces of GFs-Cu and GNPs-Cu, exacerbating the interfacial thermal resistance[64]. Therefore, it is critical to optimize mechanical bonding and ensure clean interfaces in order to improve overall TC.

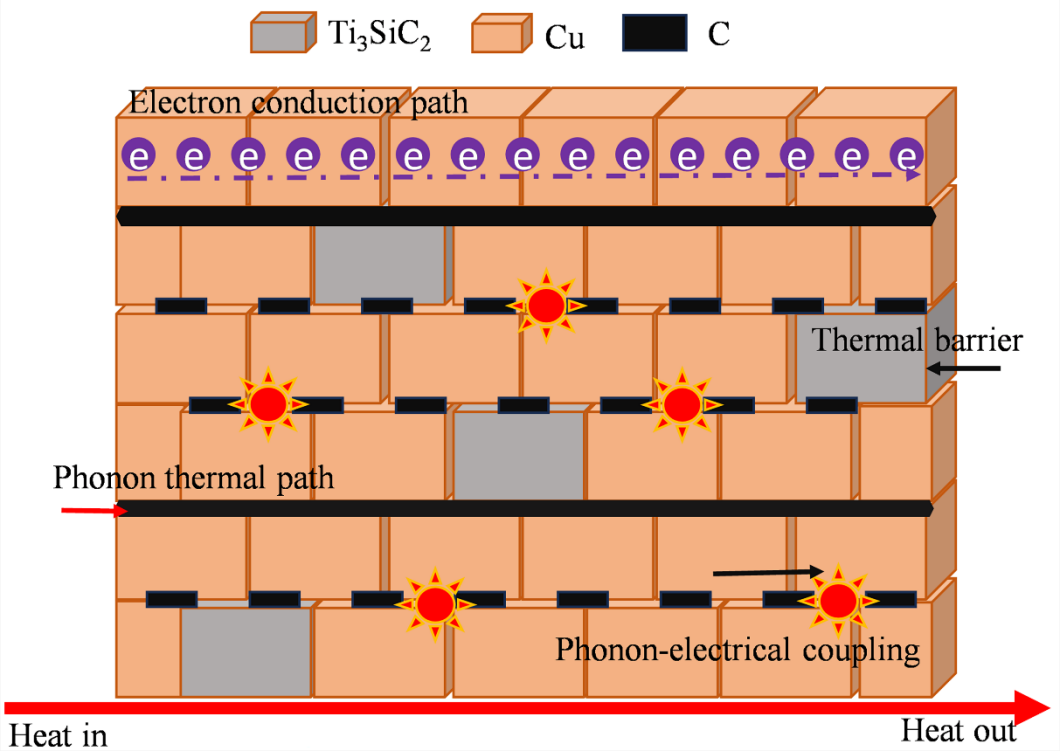

Fig. 15. Schematic of the TC mechanism of bimodal reinforced Cu/Ti_3SiC_2/C laminated-like composites.

3.4. Electrical conductivity

Fig. 16 shows that the in-plane conductivity of bimodal reinforced Cu/Ti_3SiC_2/C laminated-like composites is influenced by both the laminated-like structure and the content of GNPs. Within a certain concentration range, GNPs enhance the EC. However, when the GNP content exceeds 0.5 wt%, the positive effect on the EC diminishes. The EC of metal matrix composites is primarily determined by the movement of free electrons. This movement is influenced by structural defects, including grain boundaries, dislocations, and residual porosity[21].

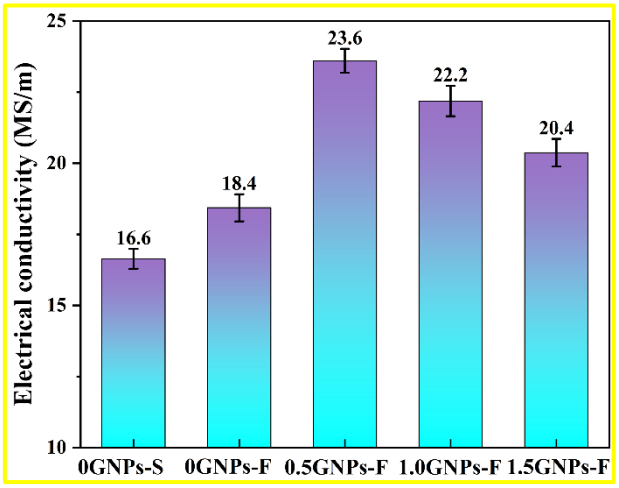

Fig. 16. Measured EC of bimodal reinforced Cu/Ti_3SiC_2/C laminated-like composites.

The conductivity changes observed in the five fabricated composites can be classified into three stages. The increase in conductivity during the first stage (composites 0GNPs-S, 0GNPs-F) is due to the laminated-like structure that promotes a more optimized particle arrangement with reduced porosity. This enhances the electron transport efficiency at the grain boundaries. In the second stage (composites 0GNPs-F, 0.5GNPs-F), the increase in EC is due to the introduction of the highly conductive phase GNPs. These GNPs are dispersed in the Cu flakes to form a directional conductive network that facilitates overall electron transport through the material. In the third stage, the EC of the composites (composites 0.5GNPs-F, 1.0GNPs-F, 1.5GNPs-F) decreases as the GNPs content increases. The XRD results show that, at this stage, the grain size of the composites becomes smaller and the number of grain boundaries increases. This is typically the location of electron

scattering and higher resistivity[20]. As the content of GNPs increases, the number of incoherent micro-interfaces formed with the matrix grains also increases. These incoherent micro-interfaces tend to have voids or are poorly bonded, which intensifies the scattering of electrons and reduces the mean free range of electron motion[65]. Furthermore, the EC of the composite is significantly reduced due to the decreased alignment of the GFs and GNPs, which are nearly disordered or randomly oriented. However, the laminated-like structure has achieved a highly aligned spatial orientation of the composites, allowing the reinforcing phases GFs and GNPs to be uniformly dispersed and form an electron-permeable network. As a result, the EC of the composites has increased. Furthermore, the reinforcing effect of Ti_3SiC_2 on the electron conduction and the hindering effect of reaction products on the electron conduction are present at all three stages. The EC of the composites is enhanced due to the good interfacial bonding, few defects, and the ultra-high conductivity of Ti_3SiC_2 itself. Conversely, the reaction products TiC and Cu_9Si are both weakly conductive phases, which will strengthen the electron scattering and reduce the electron conduction efficiency. However, as previously demonstrated, the content of such interfacial reaction products is minimal, and their influence on the EC is also negligible. Therefore, Ti_3SiC_2 has a promoting effect on the EC of the composites. In summary, the laminated-like structure has played a crucial role in achieving a uniform

dispersion of the reinforcing phases, leading to an increase in the EC of the composites. However, the weak binding at the interfaces of Cu-GFs and Cu-GNPs results in a large number of defects, limiting the contribution of the oriented percolation network to the EC.

4. Conclusions

In this study, bimodal carbon particles reinforced Cu/Ti_3SiC_2/C laminated-like composites with different GNPs contents were prepared by flake powder metallurgy and vacuum hot press sintering. The formation mechanism of the bimodal laminated-like structure and its influence on the properties of the composites were analyzed and discussed. The principal findings are as follows:

(1) The oriented assembly of GFs and GNPs was achieved through the use of flake powder metallurgy and vacuum hot press sintering. The GFs and GNPs are able to fully utilize their bimodal reinforcement properties within the laminated-like structure, thus forming unique bimodal reinforced laminated-like composites. However, due to the interaction between GFs and GNPs, an increase in the content of GNPs results in a decrease in the alignment.

(2) The mechanical properties of composites are significantly optimized by introducing a bimodal laminated-like structure. Among the composites, 0.5GNPs-F exhibited the most favorable performance, with microhardness, tensile strength, and elongation values of 125.7 HV, 276.3 MPa, and 8.4%, respectively. The FPM and GNPs facilitate grain refinement, while the high

alignment of the GFs and GNPs enhances the efficiency of load transfer and dissipation.

(3) The composites 1.5GNPs-F exhibits the highest TC (254.7 $W \cdot m^{-1} \cdot K^{-1}$), while the composites 0.5GNPs-F displays the greatest EC (23.6 MS/m). The interactions between the GFs and the GNPs form a three-dimensional reinforcing network, which leverages the planar reinforcing properties of the two materials. The network extends the thermal and electrically conductive pathways, thereby significantly improving the planar thermal and EC of the bimodal reinforced Cu/Ti_3SiC_2/C laminated-like composites.

(4) The laminated-like structure, which is bimodal, further enhances the advantages of multiphase synergistic enhancement. The efficiency of this enhancement is correlated with the alignment and continuity of GFs and GNPs. Additionally, the strong interfacial bonding contributes to the stability of load and thermoelectric carrier transfer. Therefore, optimizing the interfacial bonding of GFs and GNPs with the matrix is expected to promote the growth of composite properties.

Conflict of interest

The authors declare that they have no conflict of interest.

Acknowledgments

This work was supported by Key Laboratory of Infrared Imaging Materials and Detectors, Shanghai Institute of Technical Physics, Chinese Academy of Sciences (No. IIMDKFJJ-21-10). We would like to thank Analytical and Testing Center of Southwest Jiaotong

University for partial testing.

Data Availability statement

The data used to support the findings of this study are available from the corresponding author upon request.

Reference

[1] W. Chen, H. Zheng, L. Fan, J. Li, Z. Ding, X. Guo, F. Wu, X. Wang, P. Zheng, L. Zheng, Y. Zhang, Graphene/copper composite films: Interface regulation for enhanced electrical performance, Mater Charact, 210 (2024).https://doi.org/10.1016/j.matchar.2024.113790

[2] Y. Zhou, L. Wang, D. Kong, B. Zhang, T. Liu, Y. Yan, L. Zhang, X. Li, D. Engelberg, C. Dong, Ultra-high strength metal matrix composites (MMCs) with extended ductility manufactured by size-controlled powder and spherical cast tungsten carbide, Compos. Part A, (2024) 108194.https://doi.org/10.1016/j.compositesa.2024.108194

[3] K. Singh, V. Khanna, A. Rosenkranz, V. Chaudhary, G. Singh, S. Rustagi, Panorama of physico-mechanical engineering of graphene-reinforced copper composites for sustainable applications, Materials Today Sustainability, (2023) 100560.https://doi.org/10.1016/j.mtsust.2023.100560

[4] A. Azarniya, S. Sovizi, A. Azarniya, M.R. Rahmani Taji Boyuk, T. Varol, P. Nithyadharseni, H.R. Madaah Hosseini, S. Ramakrishna, M.V. Reddy, Physicomechanical properties of spark plasma sintered carbon nanotube-containing ceramic matrix nanocomposites, Nanoscale, 9 (2017) 12779-

12820.https://doi.org/10.1039/c7nr01878a

[5] S. Ali, F. Ahmad, P.S.M.M. Yusoff, N. Muhamad, E. Oñate, M.R. Raza, K. Malik, A review of graphene reinforced Cu matrix composites for thermal management of smart electronics, Compos. Part A, 144 (2021) 106357.https://doi.org/10.1016/j.compositesa.2021.106357

[6] H. Wei, Z. Li, J. Zou, Y. Gong, X. Li, W. Zhan, F. Li, Y. Dai, Investigation on microstructure and properties of TiCx-graphite/Cu composites fabricated by a novel in-situ reactive synthesis, Composites Communications, 38 (2023) 101494.https://doi.org/10.1016/j.coco.2023.101494

[7] A. Khamaj, W.M. Farouk, W.M. Shewakh, A.M.I. Abu-Oqail, A. Wagih, M. Abu-Okail, Effect of lattice structure evolution on the thermal and mechanical properties of Cu–Al_2O_3/GNPs nanocomposites, Ceram. Int., 47 (2021) 16511-16520.https://doi.org/10.1016/j.ceramint.2021.02.219

[8] D.-B. Xiong, M. Cao, Q. Guo, Z. Tan, G. Fan, Z. Li, D. Zhang, Graphene-and-copper artificial nacre fabricated by a preform impregnation process: bioinspired strategy for strengthening-toughening of metal matrix composite, Acs Nano, 9 (2015) 6934-6943.https://doi.org/10.1021/acsnano.5b01067

[9] M. Cao, D.-B. Xiong, Z. Tan, G. Ji, B. Amin-Ahmadi, Q. Guo, G. Fan, C. Guo, Z. Li, D. Zhang, Aligning graphene in bulk copper: Nacre-inspired nanolaminated architecture coupled with in-situ processing for enhanced mechanical properties and high electrical conductivity, Carbon, 117 (2017) 65-74.https://doi.org/10.1016/j.carbon.2017.02.089

[10] A. Wagih, A. Abu-Oqail, A. Fathy, Effect of GNPs content on thermal and mechanical properties of a novel hybrid Cu-Al_2O_3/GNPs coated Ag nanocomposite, Ceram. Int., 45 (2019) 1115-1124.https://doi.org/10.1016/j.ceramint.2018.10.001

[11] O. Güler, T. Varol, Ü. Alver, A. Canakci, Effect of Al_2O_3 content and milling time on the properties of silver coated Cu matrix composites fabricated by electroless plating and hot pressing, Mater. Today Commun., 24 (2020).https://doi.org/10.1016/j.mtcomm.2020.101153

[12] O. Güler, T. Varol, Ü. Alver, G. Kaya, F. Yıldız, Microstructure and wear characterization of Al_2O_3 reinforced silver coated copper matrix composites by electroless plating and hot pressing methods, Mater. Today Commun., 27 (2021).https://doi.org/10.1016/j.mtcomm.2021.102205

[13] T. Varol, O. Güler, S.B. Akçay, H.C. Aksa, The effect of silver coated copper particle content on the properties of novel Cu-Ag alloys prepared by hot pressing method, Powder Technol., 384 (2021) 236-246.https://doi.org/10.1016/j.powtec.2021.02.020

[14] Z. Shao, Y. Sun, W. Liu, X. Zhang, X. Jiang, Effects of Multi-Phase Reinforcements on Microstructures, Mechanical and Tribological Properties of Cu/Ti_3SiC_2/C/BN/GNPs Nanocomposites Sintered by Vacuum Hot-Pressing and Hot Isostatic Pressing, Metals, 6 (2016).https://doi.org/10.3390/met6120324

[15] F. Luo, X. Jiang, H. Sun, D. Mo, Y. Zhang, R. Shu, X. Li, High thermal and electrical properties of electroless graphene films reinforced Cu matrix laminated composites, J. Alloys Compd., 925 (2022) 166710.https://doi.org/10.1016/j.jallcom.2022.166710

[16] X. Jiang, W. Liu, Y. Li, Z. Shao, Z. Luo, D. Zhu, M. Zhu, Microstructures and mechanical properties of Cu/Ti_3SiC_2/C/graphene nanocomposites prepared by vacuum hot-pressing sintering and hot isostatic pressing, Compos. B. Eng., 141 (2018) 203-213.https://doi.org/10.1016/j.compositesb.2017.12.050

[17] H. Xiong, C. Cao, G. Chen, B. Liu, Revealing the adhesion strength and electronic properties of Ti_3SiC_2/Cu interface in Ti_3SiC_2 reinforced Cu-based composite by a first-principles study, Surf. Interfaces, 27 (2021).https://doi.org/10.1016/j.surfin.2021.101467

[18] S.-Y. Zhang, X.-B. Liu, Y. Zhu, Y.-F. Liu, Y. Meng, J. Liang, S.-H. Zhang, Stellite3-Ti_3SiC_2-Cu composite coatings on IN718 by laser cladding towards improved wear and oxidation resistance, Surface and Coatings Technology, 446 (2022).https://doi.org/10.1016/j.surfcoat.2022.128766

[19] X. Wang, K. Liu, Y. Su, X. Wang, H. Cao, A. Hua, Q. Ouyang, D. Zhang, Synergistic enhancing effect of tungsten-copper coated graphite flakes and aluminum nitride nanoparticles on microstructure, mechanical and thermal properties of copper matrix composites, Mater. Sci. Eng., A, 857 (2022) 143987.https://doi.org/10.1016/j.msea.2022.143987

[20] T. Li, Y. Wang, M. Yang, H. Hou, S. Wu, High strength and conductivity copper/graphene composites prepared by severe plastic deformation of graphene coated copper powder, Mater. Sci. Eng., A, 826 (2021) 141983.https://doi.org/10.1016/j.msea.2021.141983

[21] Y. Yang, Y. Liang, G. He, P. Luo, Graphene core–shell structure guided

functionalized interface to prepare high-strength, high-plasticity, and high-conductivity copper matrix composites, Mater. Sci. Eng., A, 847 (2022) 143349.https://doi.org/10.1016/j.msea.2022.143349

[22] J. Zhang, S.H. Shim, H. Cho, D. Lee, S.Y. Lee, J.-P. Ahn, J.H. Han, Bimodal reinforcement of graphite flake and graphene nanoplatelet in Cu matrix composites: Anisotropy of the thermo-mechanical properties and failure mechanisms, J. Mater. Res. Technol., 26 (2023) 2539-2559.https://doi.org/10.1016/j.jmrt.2023.08.060

[23] M.-Y. Seok, J.-A. Lee, D.-H. Lee, U. Ramamurty, S. Nambu, T. Koseki, J.-i. Jang, Decoupling the contributions of constituent layers to the strength and ductility of a multi-layered steel, Acta Mater., 121 (2016) 164-172.https://doi.org/10.1016/j.actamat.2016.09.007

[24] C. Shu, Z. Yao, S. Zhang, X. Tao, W. Du, Biomimetic micro-laminated structure endows cermet with excellent strength and toughness using CoCrCuFeNi as infiltration layers, Ceram. Int., 49 (2023) 39875-39885.https://doi.org/10.1016/j.ceramint.2023.09.201

[25] P. Li, X. Li, Z. Liu, L. Chen, B. Xiao, Z. Ma, Enhanced strength–ductility synergy of carbon nanotube/Al–Cu–Mg composites via introducing laminate structure and grain modification, Compos. B. Eng., 243 (2022) 110178.https://doi.org/10.1016/j.compositesb.2022.110178

[26] H. Xiao, Z.X. Huang, Z.P. Zhang, M.Z. Rong, M.Q. Zhang, Highly thermally conductive flexible copper clad laminates based on sea-island structured boron

nitride/polyimide composites, Composites Science and Technology, 230 (2022) 109087.https://doi.org/10.1016/j.compscitech.2021.109087

[27] E. Kashkarov, A. Abdulmenova, N. Pushilina, M. Syrtanov, Y. Mingazova, A. Nassyrbayev, D. Krotkevich, N. Travitzky, High temperature oxidation and thermal properties of laminated Ti_3Al (Si) C_2-TiC/Nb based composites obtained by spark plasma sintering, J. Alloys Compd., (2024) 173848.https://doi.org/10.1016/j.jallcom.2024.173848

[28] R. Shu, X. Jiang, H. Sun, Z. Shao, T. Song, Z. Luo, Recent researches of the bio-inspired nano-carbon reinforced metal matrix composites, Compos. Part A, 131 (2020) 105816.https://doi.org/10.1016/j.compositesa.2020.105816

[29] Z.-J. Hu, P. Shen, Q.-C. Jiang, Developing high-performance laminated Cu/TiC composites through melt infiltration of Ni-doped freeze-cast preforms, Ceram. Int., 45 (2019) 11686-11693.https://doi.org/10.1016/j.ceramint.2019.03.043

[30] Z. Ren, X. Gao, J. Hou, Z. Huang, T. Wang, Q. Huang, X. Liu, Achieving excellent strength-elongation synergy in corrugated Cu/Al laminated composites by flat finish roll bonding, J. Alloys Compd., 982 (2024).https://doi.org/10.1016/j.jallcom.2024.173782

[31] Y. Zhou, F. Jiang, Z. Wang, J. Chen, Microstructure characteristics and mechanical properties of Cu/Al laminated metal composites fabricated by electropulsing assisted ultrasonic additive manufacturing, Journal of Materials Processing Technology, 313 (2023).https://doi.org/10.1016/j.jmatprotec.2023.117884

[32] X. Wang, X. Jiang, H. Sun, Y. Zhang, Y. Fang, R. Shu, Microstructure and

mechanical properties of bioinspired laminated Al matrix hybrid reinforced with B_4C and graphene nanoplatelets, Mater Charact, 193 (2022) 112307.https://doi.org/10.1016/j.matchar.2022.112307

[33] T. Varol, A. Canakci, E.D. Yalcin, Fabrication of NanoSiC-Reinforced Al2024 Matrix Composites by a Novel Production Method, Arabian Journal for Science and Engineering, 42 (2016) 1751-1764.https://doi.org/10.1007/s13369-016-2295-z

[34] E. Ghandourah, H. Ahmadian, T. Zhou, A.M. Sadoun, A. Fathy, M. Atif, A. Senthil Kumar, G. Weijia, Comprehensive investigation of the impact of milling time on microstructural evolution and tribological properties in Mg-Ti-SiC hybrid composites, Mater. Today Commun., 38 (2024).https://doi.org/10.1016/j.mtcomm.2023.107835

[35] M. Akbarpour, H.M. Mirabad, M.K. Azar, K. Kakaei, H. Kim, Synergistic role of carbon nanotube and SiCn reinforcements on mechanical properties and corrosion behavior of Cu-based nanocomposite developed by flake powder metallurgy and spark plasma sintering process, Mater. Sci. Eng., A, 786 (2020) 139395.https://doi.org/10.1016/j.msea.2020.139395

[36] X. Li, B. Guo, X. Yu, C. Yang, S. Zhou, S. Cui, Z. Zhang, W. Li, Particle morphology dependence of the mechanical and electrical properties in the in-situ graphene reinforced Cu matrix composites, Compos. Part A, 179 (2024) 108032.https://doi.org/10.1016/j.compositesa.2024.108032

[37] A. Abu-Oqail, A. Samir, A. Essa, A. Wagih, A. Fathy, Effect of GNPs coated Ag on microstructure and mechanical properties of Cu-Fe dual-matrix nanocomposite, J. Alloys

Compd., 781 (2019) 64-74.https://doi.org/10.1016/j.jallcom.2018.12.042

[38] S. Guo, X. Zhang, C. Shi, E. Liu, C. He, F. He, N. Zhao, In situ synthesis of high content graphene nanoplatelets reinforced Cu matrix composites with enhanced thermal conductivity and tensile strength, Powder Technol., 362 (2020) 126-134.https://doi.org/10.1016/j.powtec.2019.11.121

[39] T. Varol, O. Güler, S.B. Akçay, H. Çolak, The evolution of microstructure and properties of Cu-Cr alloys synthesized via flake powder metallurgy assisted by mechanical alloying and hot pressing, Mater. Today Commun., 33 (2022) 104452.https://doi.org/10.1016/j.mtcomm.2022.104452

[40] R. Shu, X. Jiang, W. Liu, Z. Shao, T. Song, Z. Luo, Synergetic effect of nano-carbon and HBN on microstructure and mechanical properties of Cu/Ti_3SiC_2/C nanocomposites, Mater. Sci. Eng., A, 755 (2019) 128-137.https://doi.org/10.1016/j.msea.2019.04.002

[41] B. Pu, J. Sha, E. Liu, C. He, N. Zhao, Synergistic effect of Cu on laminated graphene nanosheets/AlCu composites with enhanced mechanical properties, Mater. Sci. Eng., A, 742 (2019) 201-210.https://doi.org/10.1016/j.msea.2018.11.016

[42] S. Peng, W. Chen, L. Fan, H. Zheng, X. Guo, P. Zheng, L. Zheng, Y. Zhang, The Preparation and Properties of In Situ Grown Oriented Nitrogen-Doped Graphene-like/Copper Composite Materials, ACS Applied Electronic Materials, 6 (2024) 1396-1404.https://doi.org/10.1021/acsaelm.3c01683

[43] K. Chu, X.-h. Wang, F. Wang, Y.-b. Li, D.-j. Huang, H. Liu, W.-l. Ma, F.-x. Liu, H. Zhang, Largely enhanced thermal conductivity of graphene/copper composites with

highly aligned graphene network, Carbon, 127 (2018) 102-112.https://doi.org/10.1016/j.carbon.2017.10.099

[44] C.-W. Nan, R. Birringer, D.R. Clarke, H. Gleiter, Effective thermal conductivity of particulate composites with interfacial thermal resistance, Journal of Applied Physics, 81 (1997) 6692-6699.https://doi.org/10.1063/1.365209

[45] X. Tian, M.E. Itkis, E.B. Bekyarova, R.C. Haddon, Anisotropic thermal and electrical properties of thin thermal interface layers of graphite nanoplatelet-based composites, Scientific reports, 3 (2013) 1710.https://doi.org/10.1038/srep01710

[46] C. Zhou, W. Huang, Z. Chen, G. Ji, M. Wang, D. Chen, H. Wang, In-plane thermal enhancement behaviors of Al matrix composites with oriented graphite flake alignment, Compos. B. Eng., 70 (2015) 256-262.https://doi.org/10.1016/j.compositesb.2014.11.018

[47] R. Zhang, F. Liu, K. Tulugan, Self-lubricating behavior caused by tribo-oxidation of Ti_3SiC_2/Cu composites in a wide temperature range, Ceram. Int., 48 (2022) 15504-15515.https://doi.org/10.1016/j.ceramint.2022.02.084

[48] Z. Wu, X. Jiang, H. Sun, Y. Li, P. Christian, L. Yang, Hybrid graphene nanoplatelets/multi-walled carbon nanotubes reinforced Cu/Ti_3SiC_2/C nanocomposites with high efficiency dispersal and strengthening through high-pressure torsion, Surf. Interfaces, (2024) 104141.https://doi.org/10.1016/j.surfin.2024.104141

[49] K. Yang, Q. Li, Q. Zhang, G. Liu, J. Wang, Y. Yang, C. Guo, J. Ni, J. Song, J. Zhang, Synergistically enhanced interface stability by graphene assisted copper surface reconstruction, Acta Mater., 226 (2022)

117638.https://doi.org/10.1016/j.actamat.2022.117638

[50] H. Yue, L. Yao, X. Gao, S. Zhang, E. Guo, H. Zhang, X. Lin, B. Wang, Effect of ball-milling and graphene contents on the mechanical properties and fracture mechanisms of graphene nanosheets reinforced copper matrix composites, J. Alloys Compd., 691 (2017) 755-762.https://doi.org/10.1016/j.jallcom.2016.08.303

[51] B. Pu, X. Zhang, X. Chen, X. Lin, D. Zhao, C. Shi, E. Liu, J. Sha, C. He, N. Zhao, Exceptional mechanical properties of aluminum matrix composites with heterogeneous structure induced by in-situ graphene nanosheet-Cu hybrids, Compos. B. Eng., 234 (2022) 109731.https://doi.org/10.1016/j.compositesb.2022.109731

[52] F. Chen, J. Ying, Y. Wang, S. Du, Z. Liu, Q. Huang, Effects of graphene content on the microstructure and properties of copper matrix composites, Carbon, 96 (2016) 836-842.https://doi.org/10.1016/j.carbon.2015.10.023

[53] Z.Y. Liu, S.J. Xu, B.L. Xiao, P. Xue, W.G. Wang, Z.Y. Ma, Effect of ball-milling time on mechanical properties of carbon nanotubes reinforced aluminum matrix composites, Compos. Part A, 43 (2012) 2161-2168.https://doi.org/10.1016/j.compositesa.2012.07.026

[54] L. Lv, X.-S. Jiang, M.-M. Zhang, H.-L. Sun, Z.-Y. Shao, N.-N. Fu, W.-T. Jin, Effect of La on microstructures and mechanical properties of Cu/Ti_3SiC_2/C nanocomposites sintered by vacuum hot-pressing and hot isostatic pressing, Mater. Res. Express., 7 (2020).https://doi.org/10.1088/2053-1591/ab5df6

[55] J. Xiaosong, W. Liu, J. Li, Z. Shao, D. Zhu, Microstructures and mechanical

properties of Cu/Ti_3SiC_2/C/MWCNTs composites prepared by vacuum hot-pressing sintering, J. Alloys Compd., 618 (2015) 700-706.https://doi.org/10.1016/j.jallcom.2014.08.221

[56] Z. Yang, J. Xu, Y. Qian, H. Liu, J. Zuo, K. Ma, M. Li, Electrical conductivities and mechanical properties of Ti_3SiC_2 reinforced Cu-based composites prepared by cold spray, J. Alloys Compd., 946 (2023).https://doi.org/10.1016/j.jallcom.2023.169473

[57] M. Wang, X. Jiang, H. Sun, Z. Wu, L. Yang, Electrical and thermal properties of bio-inspired laminated Cu/Ti_3SiC_2/C composites reinforced by graphene nanoplatelets, J. Alloys Compd., 991 (2024).https://doi.org/10.1016/j.jallcom.2024.174557

[58] K. Chu, F. Wang, X.-h. Wang, D.-j. Huang, Anisotropic mechanical properties of graphene/copper composites with aligned graphene, Mater. Sci. Eng., A, 713 (2018) 269-277.https://doi.org/10.1016/j.carbon.2015.10.023

[59] J. Fang, C. Li, F. Liu, H. Hou, X. Zhang, Q. Zhang, L. Yang, C. Xu, Z. Song, Effects of grain orientation and grain size on etching behaviors of high-strength and high-conductivity Cu alloy, Mater. Today Commun., 38 (2024) 108111.https://doi.org/10.1016/j.mtcomm.2024.108111

[60] Q. Liu, S. Tang, J. Huang, Y. Ou, J. Cheng, Y. Chen, F. Wang, Z. Lv, Microstructure and thermal conductivity of graphite flake/Cu composites with a TiC or Cu coating on graphite flakes, Mater. Res. Express., 6 (2020) 125632.https://doi.org/10.1088/2053-1591/ab5e62

[61] A. Boden, B. Boerner, P. Kusch, I. Firkowska, S. Reich, Nanoplatelet size to control

the alignment and thermal conductivity in copper–graphite composites, Nano Lett., 14 (2014) 3640-3644.https://doi.org/10.1021/nl501411g

[62] K. Chu, X.-h. Wang, Y.-b. Li, D.-j. Huang, Z.-r. Geng, X.-l. Zhao, H. Liu, H. Zhang, Thermal properties of graphene/metal composites with aligned graphene, Mater. Des., 140 (2018) 85-94.https://doi.org/10.1016/j.matdes.2017.11.048

[63] J. Wang, J.J. Li, G.J. Weng, Y. Su, The effects of temperature and alignment state of nanofillers on the thermal conductivity of both metal and nonmetal based graphene nanocomposites, Acta Mater., 185 (2020) 461-473.https://doi.org/10.1016/j.actamat.2019.12.032

[64] K. Chu, J. Wang, Y.-p. Liu, Y.-b. Li, C.-c. Jia, H. Zhang, Creating defects on graphene basal-plane toward interface optimization of graphene/CuCr composites, Carbon, 143 (2019) 85-96.https://doi.org/10.1016/j.carbon.2018.10.095

[65] J. Naseri, K. Ranjbar, M. Reihanian, Optimizing the strength and electrical conductivity of graphene reinforced Cu–Cr–Zr alloy fabricated by powder metallurgy and spark plasma sintering, Mater. Chem. Phys., 300 (2023) 127524.https://doi.org/10.1016/j.matchemphys.2023.127524